Establishing a new protocol to investigate sensory adaptation in a mouse model of Rett Syndrome

Author:
Taylor Kaban

A Dissertation Submitted in Partial Fulfillment
of the Requirements for the Degree of

Bachelor of Science with Honours

In the Department of Biology

Supervisory Committee

Establishing a new protocol to investigate sensory adaptation
in a mouse model of Rett Syndrome

Author:
Taylor Kaban

Supervisory Committee

Dr. Kerry Delaney, Department of Biology
Supervisor

Dr. Steve Perlman, Department of Biology
Honours Advisor

Dr. Craig Brown, Division of Medical Sciences
Outside Member

Abstract

This project is a continuation of Farhoomand (2021). Dr. Farhoomand studied sensory adaptation in the hindlimb to primary somatosensory cortical pathway in a mouse model of Rett syndrome to better understand the loss of MeCP2 function in neuronal circuit and sensory processing. Cortical evoked responses (CERs) to vibratory tactile stimulation of the hind limb were assessed via intrinsic optical imaging (IOS) and intracortical local field potential recordings (LFPs) before, during, and after 1 hour of repetitive vibratory stimulation at 100hz. After 1 hour, the CER was reduced by approximately 40% in both Rett mice (RTT) and wild-type mice (WT). Reduced responses persisted for at least 60 minutes in wild-type mice but recovered to 90-100% of baseline within 15 – 30 minutes in Rett mice. Analysis of this phenomenon via LFP within the test train indicated that the reduced CER was due to an increase in short term adaptation during the 7-stimulus train that was retained in the WT mice but reversed rapidly in the RTT mice. We therefore propose that the persistent sensory adaptation differences between WT and RTT that are mediated by increased short-term adaptation may reflect enhanced feedback by inhibitory elements of circuits within the sensory pathway. The lack of the adaptation to persist after continuous stimulation in the RTT mice may therefore reflect a deficit in the capacity for activity dependent plasticity to consolidate.

To determine if this is the case, this project sought to establish a new protocol to further probe this phenomenon of sensory adaptation with a larger cranial window that allows for the simultaneous recording of the CER from both hemispheres. We also seek to replace the piezo device with a new vibratory device that does not leave an artifact in the LFP data. To establish this new protocol this project sought to answer three main questions: (1) Can we reliably replace the piezo vibratory device with a motor device that is cheaper and doesn't leave an artifact in the data. We found that while there was a significant difference in the timing of the CER after stimulus offset with the motor device, there was no significant

difference in the variability of that timing, suggesting consistency with the motor device. We also found no significant difference in the sum of the peaks (mV) between the piezo device and one of the motor settings tested, and finally, we found no significant difference in the paired pulse ratio. In summary, the motor device can reliably replace the piezo device. (2) Do we see evidence for adaptation with the motor device? We found that there was evidence for adaptation, though there may be differences in the persistence of that adaptation. (3) Is there evidence for cross adaptation? We found that while there was a reduction in the CER after the adaptation phase, it wasn't statistically significant (likely due to the small sample size of N=2).

In summary, this project has established many successful aspects of a new protocol to further probe sensory adaptation. It has also paved a clear direction for the next steps in further progress towards our goal of providing a platform to understand some of the circuit level substrates of the sensory, learning, and cognitive deficits in RTT patients.

Table of Contents

Supervisory Committee ***2***

Abstract ***3***

List of Abbreviations ***7***

Acknowledgements ***8***

1: Introduction ***9***

1.1: Background on Rett Syndrome **9**

1.2: The Somatosensory Circuit Under Investigation **10**

1.3: Sensory Adaptation **13**

1.4: Rationale for the Use of IOS and LFP Methods **14**

1.5: Background on Farhoomand (2021) **15**

1.6: Rationale for This Project **16**

1.6.1: The Future Direction from Farhoomand (2021) 16

1.6.2: Rationale for Replacing the Piezo Device with a Motor Device 17

1.6.3: Why Add the Investigation of Cross-Adaptation? 18

1.7: Main Objectives **19**

2: Methods ***19***

2.1: The Mouse Model **19**

2.2 Cranial Window Procedure **19**

2.3: LFP Electrophysiology Methods **20**

2.3.1: IOS Surface Imaging to Locate the Response in the Somatosensory Cortex for Measuring the CER 20

2.3.2: Surgery for the Insertion of the electrodes 21

2.3.3: Depth of the Recording Electrode 23

2.3.4: Hindlimb Stimulation and Data Collection of LFPs 24

2.3.5: LFP Data Analysis 25

2.4: IOS Methods **26**

2.4.1: Animal and IOS Set Up 26

2.4.2: Stimulation Protocol for the Adaptation Experiment 27

2.4.3: Stimulation Protocol for Cross-Adaptation Experiment 28

2.4.4: IOS Data Analysis 29

3: Results ***32***

3.1: Comparison of motor and piezo vibratory devices within 1 animal via *in vivo* intracortical local field potential recordings **32**

3.1.1: Comparison of CER Amplitudes 32

3.1.2: A Difference in Timing of the CER 36

3.2: Comparison of the Contralateral and Ipsilateral Responses to Motor Stimulation with IOS Imaging **39**

3.3: Evidence for Adaptation with IOS Imaging **41**

3.4: Evidence for Cross Adaptation with IOS Imaging 43

4: Discussion 46

4.1: Can we replace the piezo device with a motor device? 46

4.2: Is there evidence for the same adaptation phenomenon that was found in Farhoomand (2021)? 47

4.3: Is There Evidence for Cross-Adaptation? 49

4.4: Limitations and Future Directions 49

4.5: Conclusion 50

References 52

List of Abbreviations

CER: Cortical evoked response

HL: Hindlimb

IOS: Intrinsic optical imaging signalling

LFP: Local field potential recording

LHL: Left hindlimb

MECP2: Methyl-CpG binding protein 2 gene

MeCP2: Methyl-CPG binding protein 2

PA: Persistent adaptation

PV+: Parvalbumin containing cell

RHL: right hindlimb

RTT: Rett Syndrome

SOM+: Somatostatin containing cell

STA: Short-term adaptation

TRN: Thalamic reticular nucleus

VPL: Ventral posterior nucleus of the thalamus

VSD: Voltage-sensitive dye

WT: Wild-type

Acknowledgements

First, I would like to thank Dr. Kerry Delaney, my honours supervisor for this project. It must not have been easy (to say the least) to simultaneously take on two undergraduate students who were both bold enough (or crazy enough) to attempt electrophysiology projects for their undergraduate honours projects. Dr. Delaney put himself into a busy year in agreeing to that! It has been incredibly rewarding though, and I am so grateful for his insight and for sharing his wealth of knowledge from years of dedicated experience. This work together has sparked my passion for further research, and I am excited for what graduate school and the continuation of this project will bring!

Next, I would like to thank Dr. Craig Brown and Dr. Steve Perlman for being on my committee. Dr. Perlman, you are kind, caring, and a careful fantastic scientist. Your sharp insight and pointed questions given in an empathic way have helped my growth over the year, and I'm sure my other colleagues feel the same way. Dr. Craig Brown, thank you for taking the time to answer all my questions and helping me with IOS imaging in your lab. I am excited for a continued collaboration during my graduate studies!

To my friends on the neurobiology floor, thank you for the laughs, your help with troubleshooting, and all the fun times. I am so grateful for each and every one of you. Thank you to my colleagues in the biology honours program for your feedback and friendship.

And finally, this project wouldn't have been possible without my family, close friends, and my husband. I've needed the support, understanding, love, and fun times outside of this work. I'm also grateful to all of you for listening to me babble on about this project. It has only helped me in the continuous learning of synthesizing complex topics into digestible bits of information for a more general audience. Your perspectives and questions in this regard have been invaluable!

1: Introduction

The goal of this project is to establish a new protocol to further probe the sensory adaptation differences in the hindlimb (HL) to primary somatosensory cortex circuit that were found in Farhoomand (2021) in a mouse model of Rett Syndrome (RTT). The remainder of this introduction will explain, part by part, what all of this means and why it is an important line of enquiry.

1.1: Background on Rett Syndrome

Rett Syndrome is an autism-associated neurodevelopmental disorder that affects approximately 1 out of every 10,000 live female births (Laurvick et al., 2006), and is considered one of the main causes of severe intellectual disability in girls (Percy & Lane, 2005). Female patients develop normally until around 6 – 18 months, whereby they start showing symptoms such as loss of purposeful hand movement and speech, learning and memory deficits, sensory and motor deficits, microcephaly, autonomic dysfunction, and other multisystem comorbidities that culminate in requiring 24-hour concentrated care in most cases (Lotan and Ben-Zeev, 2006; Fu et al., 2020). Due to the severity of this syndrome, continued work to better understand the mechanisms underlying symptoms will be important for the development of treatments and/or a cure.

Approximately 90% of RTT diagnoses are due to loss of function mutations of the X-linked methyl-CpG binding protein 2 gene (*MECP2)* that encodes the MeCP2 protein (Bienvenu et al., 2000). The early school of thought in RTT research was that RTT occurred in girls more than boys because it is an X linked chromosome disease, and boys only have 1 X chromosome. This would mean that if the boy were to have the mutation, he would not have a functioning *MECP2* gene and therefore no MeCP2 protein. The idea was that these boys would likely not be carried to term due to this devasting lack of MeCP2 protein, and this was the reasoning for RTT affecting mostly girls. More recent research (Gerard *et al*., 2001; Trappe

et al., 2001) has shown that the reason for the lack of RTT in males is that these mutations of *MECP2* generally occur in the father's sperm rather than in the mother's egg. This results in the disorder occurring more often in females because fathers do not give an X chromosome to male offspring.

MeCP2, a DNA-binding protein, is a multifunctional protein that is thought to act as a global transcriptional repressor (Nan *et al*., 1997). It is widely expressed in many organs, with neurons showing the highest expression levels among all MeCP2 expressing cells. (Zachariah et al., 2012). Unsurprisingly then, MeCP2 has been shown to be important for brain development and function, especially in terms of regulating synaptic and neuronal plasticity in the brain (Na et al., 2012). Since loss of function of MeCP2 is the primary cause of RTT, research on RTT has focussed much of its efforts on the effects of that loss of function on brain circuit functioning. The general hypothesis is that the neurological deficits of RTT patients arise because of a failure in synaptic and circuit development, functioning, and maintenance (Bellini et al., 2014). The current project focusses on sensory adaptation in the HL to primary somatosensory cortical circuit to further the understanding of the role of MeCP2 in circuit functioning and sensory processing under this line of reasoning.

1.2: The Somatosensory Circuit Under Investigation

In this project we stimulate the HL with a vibratory stimulation and record the resulting cortical evoked response (CER) in the HL primary somatosensory cortex. The pathway responsible for bringing this sensory information from the periphery (HL) to the HL primary somatosensory cortex in the mammalian nervous system is The Dorsal Column-Medial Lemniscal System, which conveys tactile and proprioceptive information up to the primary somatosensory cortex. With the vibratory stimulation to the paw, we are most likely activating two main classes of mechanoreceptors: (1) the cutaneous mechanoreceptors in glabrous (non-hairy) skin, which are specialized to receive and transmit tactile information derived from

external stimuli, and (2) the proprioceptors, which are specialized mechanoreceptors responsible for providing information about mechanical forces arising from within the body itself. This proprioceptive information gives detailed and continuous information about the position of the joint, limb, and the body in space. (Purves *et al*. [Chapter 9], 2018).

Figure 1 below depicts a simplified schematic of the dorsal column-medial lemniscal pathway that brings sensory information from the HL up to the primary somatosensory cortex. Note that it's simplified because there are collaterals to adjacent spinal segments not shown, and the proprioceptive information has another route not shown that brings information to the cerebellum via the spinocerebellar tract. Therefore, while the proprioceptive path is technically different, it still follows the dorsal column pathway and meets back up with it to synapse in the ventral posterior lateral nucleus of the thalamus (VPL).

The dorsal column-medial lemniscus pathway includes three types of neurons along the path. The first are the primary neurons. These neurons have a soma (cell body) located in the dorsal root ganglion, and they transmit the sensory inputs from the mechanoreceptors to the spinal cord. These are labelled 'Dorsal root ganglion cells' on figure 1 below. The afferent fibers of these primary neurons travel up the gracile tract and synapse with secondary neurons in the gracile nucleus of the medulla (brainstem). The afferents of these secondary neurons (in blue in Figure 1) decussate (cross-over) and travel up the contralateral side of the body to synapse with the third type of neuron in the somatosensory portion of the thalamus, the VPL. This third type (in red), called the thalamic relay neurons, provide excitatory input to the primary somatosensory cortex by synapsing with both excitatory and inhibitory neurons within layer 4.

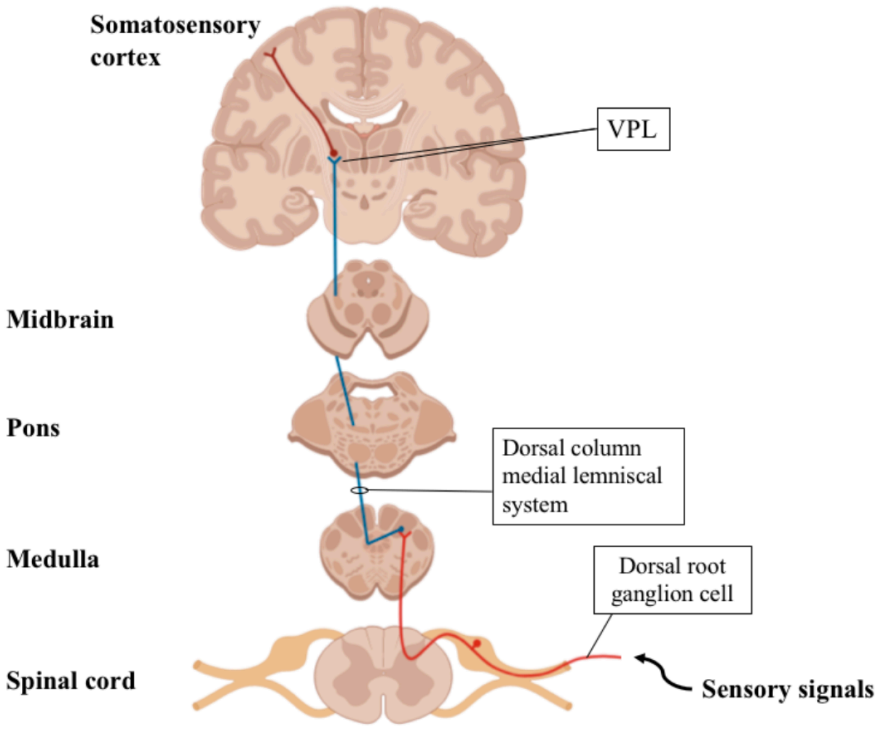

Figure 1: The dorsal column-medial lemniscal pathway. Sensory signals brought in by mechanoreceptors are sent through the primary neurons (dorsal root ganglion cells) to synapse with secondary neurons in the medulla (brainstem). From there, the information is sent to synapse with third-order neurons in the somatosensory portion of the thalamus, the VPL. From the thalamus, these signals project predominantly to layer 4 of the primary somatosensory cortex.

From here, things get a little bit more complex. The circuit mentioned above constitutes the feedforward projections from the periphery up into the cortex through the thalamus. There are also extensive feedback projections to the thalamus from the cortex. This is illustrated in Figure 2 below. All of this constitutes the thalamocortical circuit. For example, there are feedback projections from layers 5 and 6 of the cortex both going directly to the thalamus, and indirectly to the thalamus via the thalamic reticular nucleus (TRN) (Whitmire and Stanley, 2016). The TRN, which in rodents provides inhibition to all thalamic nuclei (Arcelli *et al.,* 1997) contains predominantly inhibitory neurons, specifically parvalbumin (PV+) and somatostatin (SOM+) cells (Clemente-Perez *et al*., 2017; Houser *et al*., 1980). The thalamus therefore is integrating the raw sensory feedforward information with the descending feedback signals from layers 5/6 and the TRN and finally transferring that integrated sensory information back to the brain

(Groh *et al*., 2014). Interestingly, MeCP2 is expressed in both PV+ cells and SOM+ cells, and there is mounting research implicating dysfunction in these cells with causing aspects of the RTT phenotype (Ito-Ishida *et al.,* 2015). This adds evidence to support the continued investigation of this circuit.

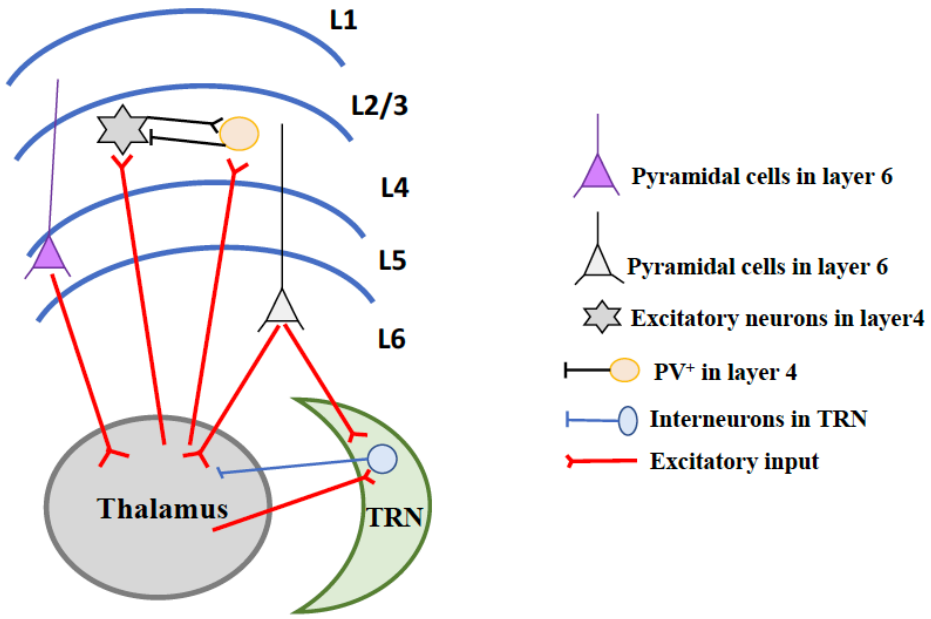

Figure 2: The feedforward and feedback projections of thalamocortical circuitry. The feedforward projections move from the thalamus to layer 4 of the primary somatosensory cortex. Feedback projections predominantly come from layers 5 and 6 of the cortex that synapse both directly back onto the thalamus and indirectly to the thalamus via the TRN, which is predominantly inhibitory in nature. In this way, the thalamus is integrating both feedforward and feedback pieces of information and sending this integrated information back to layer 4.

1.3: Sensory Adaptation

Sensory adaptation is a ubiquitous property of all sensory pathways (Whitmore and Stanley, 2017). In short it is some change in the nervous system that is caused by previous experience. In this way, you can think of it as a very simple form of memory within the nervous system. The sensory adaptation that we focus on for this project is a form of activity-dependent synaptic plasticity, which is generally defined as a change in connection strength between a neuron and its target cell that is dependent on their being

activity in the presynaptic neuron. Generally, these short-term changes to synapses are caused by repetitive stimulation of the presynaptic neuron (Zucker and Regehr, 2002). We study two forms of sensory adaptation in this project. The first is a short-term sensory adaptation (STA) that develops during a short train of 7 stimuli, and the second form is a persistent form of adaptation (PA) that is seen as a decrease in the cortical evoked response (CER) lasting an hour or more following many minutes of repeated sensory stimulation.

1.4: Rationale for the Use of IOS and LFP Methods

Both this project and Farhoomand (2021) employ the use of intrinsic optical signalling (IOS) and intracortical local field potential recordings (LFP). IOS makes use of the tight coupling between neural activity and blood flow in the brain. The brain consumes a large amount of energy but lacks a reservoir to store fuel for use when needed, so it gets its energy source 'on the fly' from blood supply. The brain and vascular system are therefore set up such that blood flow is very precise in timing and location to areas of neural activity (Iadecola 2017). Functional imaging methods make use of this tight coupling by measuring the blood oxygen level as a correlate of neural activity.

IOS is one such functional imaging method that uses this. It measures changes in light reflectance from the cortex when the cortex is illuminated by red light, and these changes in light reflectance are attributed to changes in blood volume, deoxygenated hemoglobin concentration, and/or the light scattering of tissue (Chen-Bee *et al.* 2000). This allows us to measure neuronal activity by correlating it with blood flow changes. This method was chosen due to the non-invasive nature of it, and the strength of its ability to locate neural activity in space. The non-invasive nature makes it a great method to add the potential of a treatment protocol, whereby you can measure both before and after treatments within the same animal.

A downside of a method that uses blood flow changes as a correlate for neural activity is the fact that you are not measuring neural activity directly, and the activity you measure has poor temporal resolution. Therefore, we also use LFP. This measures neural activity directly and has high temporal resolution. In these projects, both IOS and LFP methods are used *in-vivo* in a living mouse. This means that the brain remains intact. Both methods together in this way can therefore elucidate circuit level functioning within a living organism. This is important when considering the study of a complex syndrome like RTT.

1.5: Background on Farhoomand (2021)

Farhoomand (2021) studied the two forms of sensory adaptation mentioned above by stimulating the left HL (LHL) with a vibratory piezoelectric device and assessing the resulting CER in the contralateral hemisphere with both IOS and LFP *in vivo.* The CER was assessed with test vibrations of 10Hz both before, during, and after an hour of repetitive stimulation at 100Hz of the LHL. This protocol was assessed in presymptomatic RTT female, as well as symptomatic RTT male and female mice as compared to age-matched wild-type (WT) mice.

After 1 hour of repetitive stimulation, the resulting CER to test vibrations was reduced by approximately 40% in RTT and WT mice in both methods (IOS and LFP). Recovery of the IOS responses were tested every 15 minutes following the repetitive stimulation. The reduced responses persisted for at least 60 minutes in the WT mice but recovered to 90-100% of the normal CER magnitude within 15 – 30 minutes for the RTT mice. The LFP protocol was set up such that the vibratory test trains included 7 brief vibratory pulses at 10Hz. The analysis of this LFP data indicated that the reduced CER response during and immediately after the continuous vibratory stimulation resulted primarily from an increase in

short-term adaptation (STA) during the 7-stimulus test train that was retained more long-term in the WT but reversed rapidly in the RTT mice. In this way, the WT mice showed PA, while the RTT mice did not.

The proposal from Farhoomand (2021) is that the PA is mediated by increased STA, and this may reflect enhanced feedback by inhibitory elements of circuits within the sensory pathway. This assertion of there being a potential enhancement of feedback by inhibitory elements is supported by other RTT research showing changes in the excitatory/inhibitory balance all throughout the RTT brain (see Li, 2022 for different brain-region specific changes to the excitation/inhibition balance across RTT research). The rapid recovery of the responsiveness to repetitive tactile stimulation might therefore reflect a deficit in the capacity for activity dependent plasticity to consolidate. Understanding this simple form of plasticity may therefore provide a platform to understand some of the circuit level substrates of learning and cognitive deficits in RTT patients.

1.6: Rationale for This Project

1.6.1: The Future Direction from Farhoomand (2021)

The key difference that Farhoomand (2021) found in the HL to primary somatosensory cortical circuit between RTT and WT mice was that while RTT and WT mice showed equal reductions in the CER after an hour of vibratory stimulation, the STA persisted for at least an hour in the WT mice, but rapidly reversed in the RTT mice. In this way, the STA did not have a chance to consolidate into a more persistent form (PA) in the RTT mice. This shows that there are differences in the sensory circuits involved in processing this information across WT and RTT mice.

What we are trying to do next is determine where in the circuit that the sensory adaptation is occurring. As was seen in Figures 1 and 2, there are many synapses within the circuits that process this

information. Farhoomand (2021) investigated this in the sciatic nerve and found that there was not peripheral sensitization occurring there, which supports the idea that the adaptation phenomenon is occurring in the CNS rather than the PNS. We do not yet know where in the CNS this is happening. It could be in multiple synapses, or predominantly just one. It could be a higher order process up in the cortex and/or thalamus, or it could be in the brainstem, or it even could be a cascade of adaptation from the HL up to the cortex. The difference in the rate of recovery between RTT and WT mice could also be due to different sites of STA, with the difference in rate of recovery reflecting different mechanisms of adaptation altogether.

The goal of this project is to establish a new protocol that will allow us to further probe these differences to hopefully uncover the answer to these questions. The answer to these questions may give us insight into more pervasive and underlying mechanisms, which could help with potential treatments for RTT. This new protocol involves replacing the piezo vibratory device with a motor device and using a larger cranial window that allows us to record the CER simultaneously from both hemispheres. This will allow us to look at whether the adaptation phenomenon that was found in Farhoomand (2021) crosses over to the opposite HL to cortical somatosensory circuit.

1.6.2: Rationale for Replacing the Piezo Device with a Motor Device

There are three main reasons for the desire to replace the piezo device with a motor device: (1) the motor device is a couple orders of magnitude cheaper in price than the piezo device (around ~2-4$ per device rather than ~200+$ for the piezo). Both devices eventually need to be replaced to maintain equal levels of power across time, so the cost of using the motor is much more economical. (2) the piezo device leaves an artifact in the LFP trace, while the motor device does not. The artifact for the piezo device occurs on top of biology, and this means that you lose some of the biological data that's mixed in with the artifact. The motor device does not have that problem, and this could allow us to consider different avenues of

analysis with the motor traces since the whole motor trace is therefore just biology. (3) Replacing the piezo device with the motor device might allow us to train the mice such that we could employ IOS without anesthesia.

Isoflurane, the anesthesia we use, is known to alter brain activity evoked by external stimulation (Paasonen *et* al., 2016), and known to alter the hemodynamic response (Martin *et* al., 2006) in rats. We do not use rats, but our methods do rely on brain activity evoked by external stimulation (HL vibratory stimulation) and the hemodynamic response (the basis of IOS imaging), and they include multiple hours under isoflurane for the adaptation experiments. Running the adaptation experiment in awake mice was not possible in Farhoomand (2021) because the piezo device is intensive and loud.

The motor device is not as intensive or loud as the piezo device, so the ability to use it instead of the piezo device might allow for the same experiments to be run in awake mice instead of in lightly anesthetized mice. We first need to determine if the motor device causes the same form of adaptation and differences across WT and RTT mice before we can replace the piezo device, and that is where this project comes in.

1.6.3: Why Add the Investigation of Cross-Adaptation?

Across species, there is evidence that although the primary response to sensory activity is in the contralateral hemisphere, there is recordable activity in the ipsilateral hemisphere too (Pidoux and Verley 1979, Tommerdahl *et al*. 2005, Hllushchuk and Hari 2006, Lipton *et al.* 2006, Ferezou *et al. 2007,* Plomp *et al*. 2017, Song *et al.* 2018, Pala and Stanley 2021). These responses in the ipsilateral hemisphere have been shown to be mainly mediated by corticocortico projections via the corpus callosum (Pidoux and Verley 1979, Fabri *et al*. 1999). With this in mind, we want the ability to measure these ipsilateral

responses during adaptation too. Do these ipsilateral responses adapt? If they do, does this adaptation also cross over into the opposite circuit? The answers to these questions will help us pinpoint where exactly the sensory adaptation evident in Farhoomand (2021) is occurring within the circuit.

1.7: Main Objectives

For establishing a new protocol, this project has three main questions it seeks to answer:

1) Can we reliably replace the piezo device with the motor device?

2) Is there evidence for the adaptation found in Farhoomand (2021) with the new motor device?

3) Is there evidence for cross-adaptation?

2: Methods

2.1: The Mouse Model

The RTT mouse model that we use in the lab is a mouse line that lacks exon three on the *Mecp2* gene. These mice are housed in 12hr/12hr light/dark cycles. We breed heterozygous females (*Mecp2*$^{+/-}$) with WT (C57BL/6) males. The initial heterozygous RTT females were provided by UC Davis MMRRC (*Mecp2*$^{tm1.1Jae}$). Our cross of heterozygous females with WT males results in offspring that are; (1) WT male, (2) RTT male (*Mecp2*$^{-/y}$), (3) WT female, and (4) heterozygous female (*Mecp2*$^{+/-}$). This project used female two-month-old WT offspring from this line to establish the new protocol for adaptation and cross-adaptation experiments with the motor device. Once this protocol is established, RTT mice will be used to compare across to age-matched WT mice. PCR was used to confirm the genotype of the animals. 8 WT female mice were used for this experiment.

2.2 Cranial Window Procedure

Before the procedure, an 8mm glass coverslip was glued to a cranial window ring with KrazyGlue™. This was done an hour before the procedure began to allow the glue to fully dry. The glass coverslip did not

fully cover the bottom of the ring. For the procedure itself, each animal was anesthetized with 1.5% isoflurane: air. The depth of anesthesia was monitored by the response to a toe pinch. The animal's body temperature was monitored with a rectal probe and maintained between 36.5°C to 37°C by a thermostatically controlled heating pad. A circular region of the skull with bregma approximately in the center was exposed and thoroughly cleaned. A thin layer of clear drying dental cement (C&B-Metabond™) was applied over the exposed and intact skull, and the ring and glued glass coverslip was gently placed over the region. The dental cement dries clear and locks the cranial ring and glass coverslip in place on top of the skull. Once the glue is dry, the vessels on the surface of the brain become clearly visible through the glass coverslip. This method allows the cranial window to be non-invasive as compared to other methods that thin and/or remove the skull for imaging. This results in quicker recovery times for the mice. The cranial window procedure was completed at least 3 days prior to the imaging sessions to give the mice ample time for recovery from the anesthesia. Another benefit of the intact skull method for this cranial window procedure is that keeping the skull intact minimizes heartbeat-induced and breathing related brain movement and therefore helps to reduce noise.

2.3: LFP Electrophysiology Methods

2.3.1: IOS Surface Imaging to Locate the Response in the Somatosensory Cortex for Measuring the CER

To be able to precisely place a recording electrode in the LHL contralateral somatosensory cortex to measure the CER from vibratory stimulation, a surface image and short IOS session was necessary. This IOS session occurred 3 days before the electrophysiological recording session. The same stimulation and recording process that is explained in more detail below under IOS methods was used here. In summary, the LHL was stimulated with the vibratory device, and the response in the contralateral (right) hemisphere was collected. The strongest location of that response was superimposed on a surface image of the brain through the cranial window via ImageJ software. The surface image was collected with green light

(≈550nm) with the use of a 2x objective lens (NA 0.14). This allowed us to landmark the position where the electrode would need to be placed for successful electrophysiological recording of the CER. A visual depiction of this process is shown below in Figure 3.

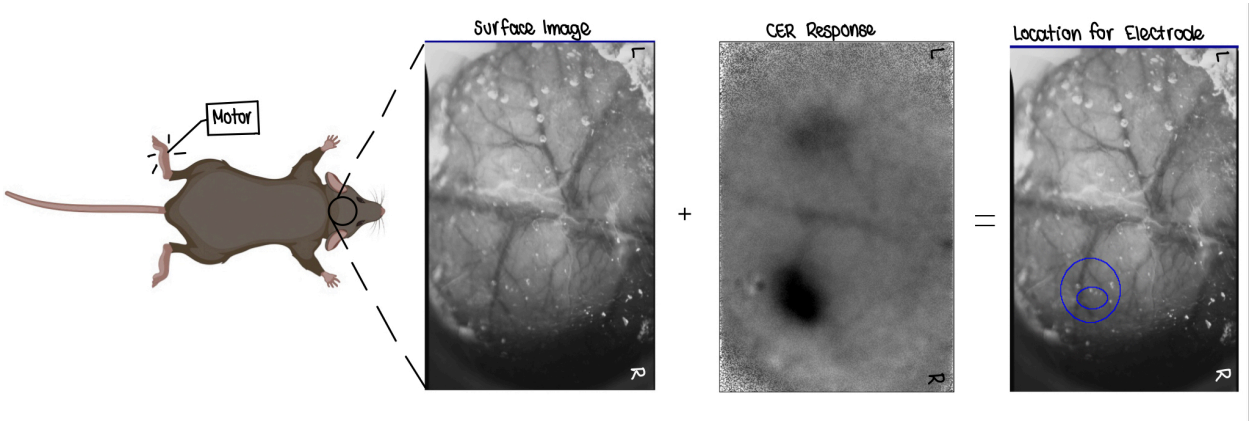

Figure 3: Visual depiction of the process for locating where the recording electrode needs to be inserted into the LHL somatosensory cortex for electrophysiological recording of the CER response. First, a surface image of the cerebral blood vessels is collected through the cranial window with green light (≈550nm) and a 2x objective lens (NA 0.14). Next, the LHL was stimulated with the motor device and the resulting CER response is recorded. This is seen in the middle image labelled 'CER Response'. Finally, a circle is drawn around the response, added to an ROI manager in ImageJ, and then superimposed onto the surface image. The outer blue ring is the location of the full response. The second inner blue ring is the location of the strongest response. The recording electrode is inserted into the brain at the location of the inner blue circle.

2.3.2: Surgery for the Insertion of the electrodes

During the surgery the animals were anesthetized with 1.5% isoflurane: air, and just like the previous surgical methods, the toe pinch method was used to monitor anesthetic depth. Body temperature was monitored with a rectal probe and maintained between 36.5 and 37°C by a thermostatically controlled heating pad. Two electrodes then needed to be inserted into the brain. A reference electrode (0.005'0.007' Teflon™ coated Ag-AgCl electrode) was inserted into the left posterior hemisphere (opposite hemisphere to the recording side) of the cerebral cortex. The coordinate for this placement was bregma -4.16mm, and lateral 1.5mm. This electrode was secured with cyanoacrylate glue. Next, a dental drill was used to lightly thin the skull over the area where the electrode needed to be inserted (the inner blue circle in Figure 3 above) until thin cracks appeared in the skull that were sufficiently sized for

the recording electrode. The recording electrode (borosilicate glass capillary with O.D. = 1.5mm, I.D. = 0.86mm, Sutter Instruments) was pulled to an ≈ 2.5µm tip diameter with 1.5MW resistance. It was then filled with brain buffer (NaCl 135mM, KCl 5.4mM, HEPES-Na salt 5mM, MgCl2 0.5M, CaCl2 0.5M, PH=7.35) and inserted into the brain at a depth of 350µm from the surface of the brain. An Ag-AgCl wire was also inserted under the skin at the back of the animal's neck to function as a ground for the animal. This set up of electrodes is illustrated below (Figure 4).

Once the electrodes were placed in the animal, the anesthetic level was dropped to 1% isoflurane: air. Body temperature was monitored with a rectal probe and kept tighter than the other surgical procedures at 36.5°C by a feedback-controlled heating pad. A drop of mineral oil was applied to the exposed brain to keep the area moist. The animal was given 30 minutes to acclimate to the set-up before recording began.

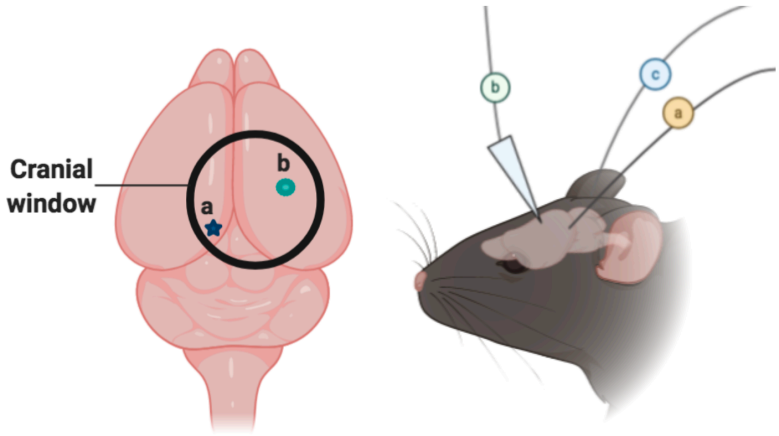

Figure 4: Location of electrodes for LFP recording (from Farhoomand 2021). Note that with my set up, the only difference to this diagram is the fact that my cranial window is larger (8mm instead of 3mm glass coverslip as was done in Farhoomand (2021). This means that my cranial windows are more centered. The 'a' electrode is the reference electrode, 'b' is the recording electrode, and 'c' is the ground wire.

2.3.3: Depth of the Recording Electrode

The recording electrode was inserted 350µm into the brain. The decision of this depth for recording comes from Farhoomand (2021). In that project, the best depth for recording was determined by recording the CER in response to HL stimulation at different depths (from 100 – 800 µm into the brain). The maximum response amplitude for the CER was recorded between 300 – 400µm into the brain. The middle of this maximum response depth was then chosen (350µm). The results of are illustrated in Figure 5 below (which is a figure from Farhoomand 2021).

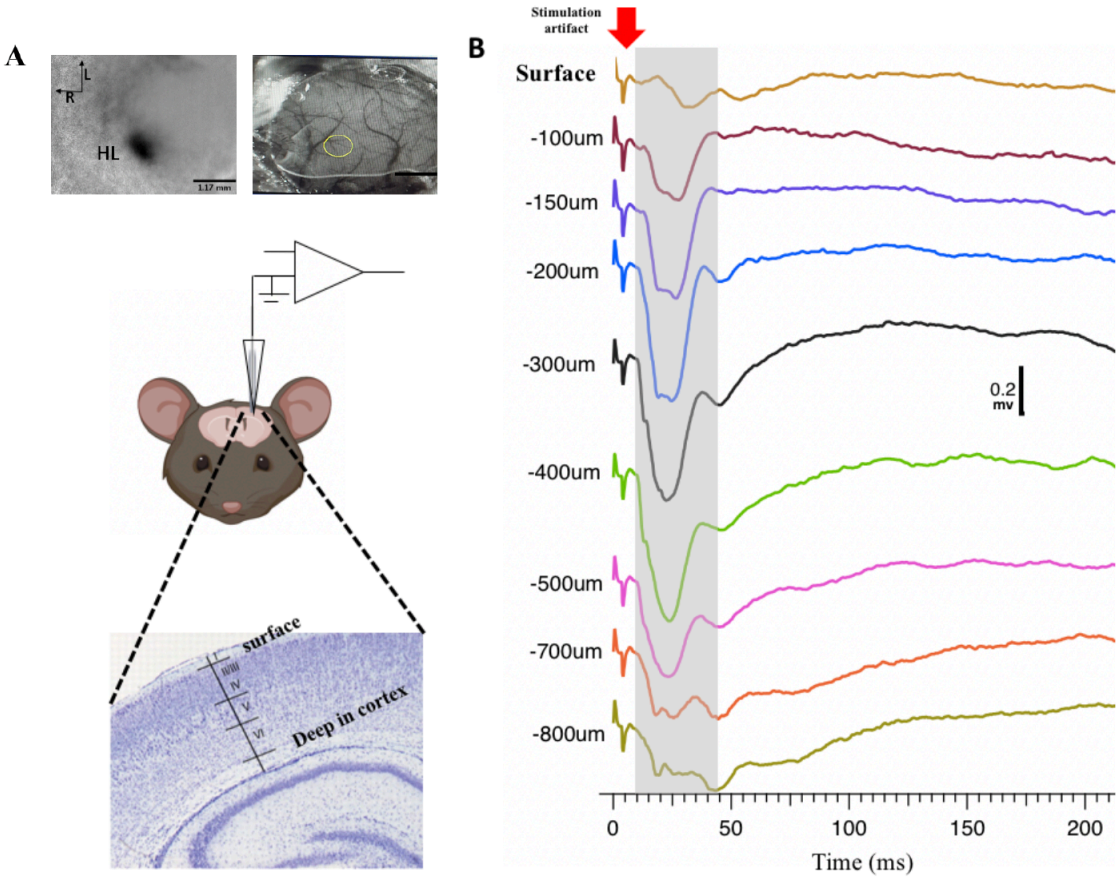

Figure 5: Determining the best depth into the brain for the recording electrode (from Farhoomand 2021). **(A):** Depicts the process of using IOS and the surface image to map the location of where the electrode needs to be placed (in the center of the LHL receptive field). The lower half of (A) shows a visual depiction of the depth of the cortex. **(B):** Shows the depth experiment. The response is small on the surface and is larger as the electrode is inserted deeper. The maximal response occurs between 300 – 400µm below the surface of the brain. Once beyond 400 µm, the response gets smaller again. The red arrow shows the stimulation artifact (from piezo), and the maximum response is seen around 20ms after the stimulation offset.

2.3.4: Hindlimb Stimulation and Data Collection of LFPs

For the LFP recordings, only the LHL was stimulated, and recordings were done in the right contralateral hemisphere. This LFP setup used both the piezo and motor devices to compare the resulting CERs from stimulation of each. For piezo, one end of a 2.5cm long pencil led was glued between toe 3 and 4 on the top side of the paw. The other end of the pencil led was attached to the end of a piezoelectric device. For the motor device, the motor was taped to the bottom of the paw with double sided sticky tape. Two settings for the motor were compared: (1) Motor60mA. Each stimulation for this setting had a 30ms duration, and the voltage was 4.28V to cause 60mA of current to activate the motor. (2) Motor70mA. Each stimulation was also 30ms in duration, and the voltage was 5V to cause 70mA of current to activate the motor. Note that we also tested a third voltage output (3.57V to cause 50mA of current), but this setting was not able to run the motor, so it was not included.

To generate the CER, the vibratory stimulation was applied as a 7-stimulus train, where each stimulation came in at 10Hz for a total of 700ms across the whole train. That stimulation paradigm was then repeated for a total of 20 times for 1 sample collection, and those 20 raw traces were averaged for a single measurement of the CER response to each of the 7 stimulations within the train. 5 rounds of this were completed for each of the three vibratory settings (piezo, motor60mA, and motor70mA). A final average of those 5 rounds was computed in IgorPro for each setting to allow for comparisons within 1 animal. To collect the LFPs, A 1700 differential amplifier (A-M system) was used with signals amplified by 1000x, filters set at 0.1Hz for lowpass and 1KHz for high pass, and digitized with 20KHz using an Instrutech18™ by ChartMaster™. Data were then transferred to IgorPro™, and analysis was done using the NeuroMatic package. Note that only one animal's LFP responses was researched in this way due to time constraints of this project. More animals will be needed to test across animals to ensure the patterns found in this one animal are repeatable in other animals.

2.3.5: LFP Data Analysis

The first step to measuring the peak LFP amplitudes of the CER response was collecting information for the x position of the maximum deflection point. Once that was collected for each of the 7 peaks within the 7-stimulus train, windows could be set up in the NeuroMatic™ package for the calculation of each peak amplitude for each of the average of the raw traces (5 for each vibratory device) and for the average of the averages for each vibratory device.

To calculate, an average of 15ms of brain activity immediately prior to stimulus onset was subtracted from the average magnitude value (in mV) of the wave from the max deflection point ± 1ms around that maximum deflection point. This process is why the x position of the maximum deflection point was calculated first.

This method of analysis has one slight change from Farhoomand (2021). In her project, a baseline average of 30ms was used for the subtraction. I needed to use 15ms because the motor device resulted in a delay of the position of maximum deflection. If I were to have used 30ms with the motor device analysis, I would have been subtracting a portion of the previous peaks activity as a baseline value, and that would have biased the entire set of results. To avoid this, I shortened the baseline average time to 15ms to keep it consistent across vibratory device analysis. Figure 6 below from Farhoomand (2021) depicts this process for the piezo device (though it is the same process for the motor devices). Note again that the only difference in analysis for my project is that the baseline activity is 15ms rather than 30ms.

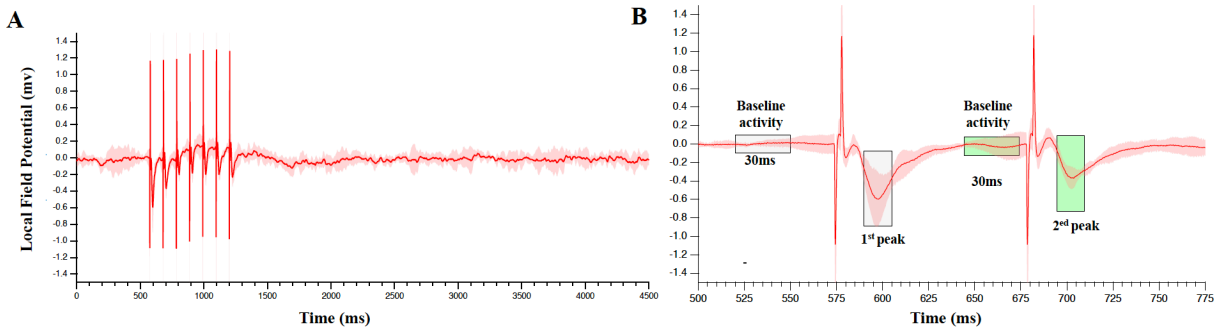

Figure 6: Data analysis process for the peak amplitude calculation of the LFPs (Figure from Farhoomand 2021). **(A):** An example trace of the average of 20 raw traces. There were 5 of these in total for each vibratory device. **(B):** The baseline activity measurement was subtracted from the average from the maximum deflection point ± 1ms of data around that maximum deflection point. Note that in Farhoomand 2021, the baseline was an average of 30ms, but for my project the baseline average used was 15ms of data.

2.4: IOS Methods

2.4.1: Animal and IOS Set Up

For IOS sessions, animals were anesthetized at 1.2% isoflurane: air. Body temperature was tightly regulated at 36.5 ± 0.5°C with a rectal probe and a thermostatically controlled heating pad. Once the animal was in place and sufficiently anesthetized (as monitored by a toe pinch), the motor device was set up with double sided sticky tape under the paw.

For the adaptation experiments, just one motor was taped to the bottom of the LHL. With the cross-adaptation experiments, a second motor was taped to the bottom of the RHL. IOS uses red light (~620nm) to record the activity of the CERs in the hemispheres through the cranial window. A 2x objective lens (NA 0.14) was used. As described in Chen-Bee *et al*., (2000), the imaging plane was focussed ~300 – 350µm below the cortical surface to minimize measurement contribution from surface blood vessels.

Each stimulation lasted 1 second, and brain activity was recorded for 3 seconds in total, with 1 second of pre-stimulation activity, 1 second of activity during stimulation, and 1 second of brain activity

after stimulation offset. This round of 1 stimulation constitutes 1 trial, and 5 of these trials were repeated with an inter-trial-interval of 14 seconds for an average measurement. 14 seconds are necessary between trials because IOS measures changes in light reflectance from the illuminated cortex (from the red light) attributed to changes in blood flow/concentration (predominantly deoxygenated hemoglobin), which is itself strongly correlated with neuronal activity. These blood flow changes take 14ms to return to baseline levels.

The reason for collecting only 1 second of brain activity after stimulation offset is due to previous research showing a faster change in deoxygenated hemoglobin following sensory stimulation from fast oxygen consumption of activated neurons as compared to the slower change in blood flow that occurs in the large blood vessels (Mayhew *et al*., 1999; Nemoto *et al*., 1999; Vanzetta and Grinvald, 1999). This gives us the best chance of collecting the change in blood flow data as a change in light reflectance from the active neurons without introducing bias from the large overlying blood vessels.

2.4.2: Stimulation Protocol for the Adaptation Experiment

The stimulation protocol for the adaptation experiments used the motor at 70mA of current, and a visual depiction of this protocol is shown in Figure 7). The motor device was taped to the bottom of the LHL paw. Two baseline measurements were taken, one labelled as -15 minutes, and the other one at 0 minutes (15 minutes apart). These were 10Hz 1 second stimulations repeated 5 times with a 14ms interval between them. Then, there was 45 minutes of continuous stimulation to the LHL that was set up as 10Hz stims for 1 second every 6 seconds. This was the adaptation period (in blue highlighter on FigureX below). After the 45 minutes, there was a 2-minute period of rest before taking the adaptation measurement (collected in the same manner as the baseline measurements). The animal was given a further 45 minutes of rest before taking the final recovery measurement (again, the same as the other measurements at 10hz). The recovery measurement was used as a control to ensure that any reduction that might happen

in the adaptation measurement is not simply explained by reduction in health or response in the animal overall. Seeing a recovery of the adaptation measurement gives evidence that adaptation is indeed happening.

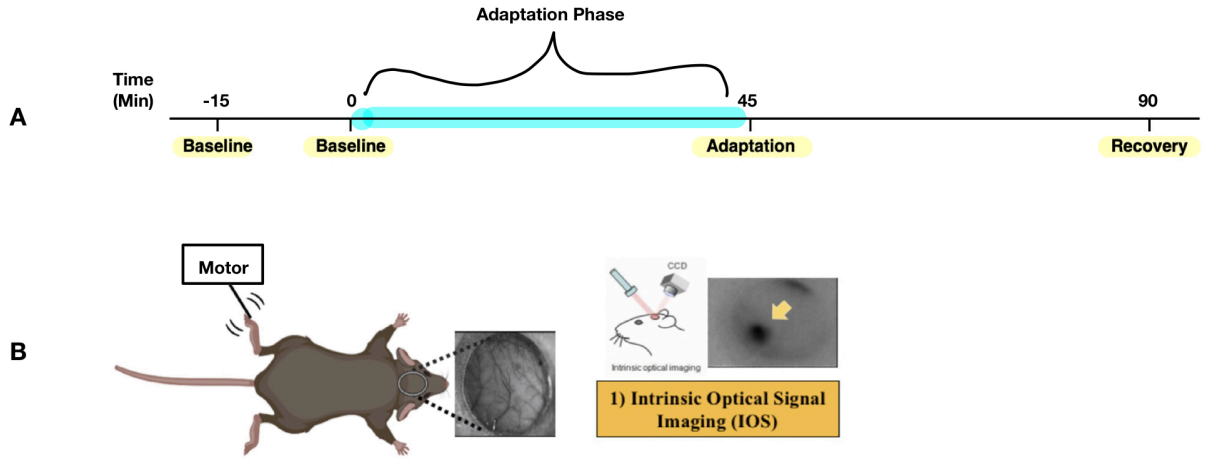

Figure 7: Stimulation protocol for the adaptation experiment (some aspects of the figure are adapted from Farhoomand 2021). **(A):** protocol in visual form. The yellow highlighted text represents the 4 measurements (2 baseline, 1 adaptation, and 1 recovery). Two baseline measurements were taken 15 minutes apart. The blue highlighter represents the adaptation phase, where continuous stimulation of 10hz for 1 second every 6 seconds occurred. The adaptation measurement came after the adaptation phase + 2 minutes of rest. The recovery measurement occurred 45 minutes after the end of the adaptation period. **(B):** Image showing the motor placement, cranial window, and IOS method of collecting each measurement.

2.4.3: Stimulation Protocol for Cross-Adaptation Experiment

Establishing a new protocol with an 8mm glass coverslip cranial window has allowed the possibility of recording CERs from HL vibratory stimulation in both hemispheres simultaneously. This has allowed us to ask the question of whether the adaptation that was present in Farhoomand (2021) crosses over into the opposite hindlimb circuit. To test this, we needed two motors, one taped to the bottom of the paw of each HL. We then needed to adapt one circuit (the LHL to contralateral (right) hemisphere), and then test whether that adaptation crossed over by stimulating the RHL and recording from the contralateral (left) hemisphere. We therefore needed a baseline measurement for each circuit. To do so, we recorded two baseline measurements from LHL stimulation, both 15 minutes apart and in the same manner as the

adaptation experiment (1 second 10Hz stimulations for each). We then took two baseline measurements for the RHL stimulation that were also 15 minutes apart. After that final baseline measurement, we stimulated the LHL for 45 minutes. Once the 45 minutes was up, we stopped the continuous stimulation, waited 2 minutes, and then stimulated the RHL and recorded the CER. We then waited 5 minutes and recorded from LHL stimulation. This measurement was a control to make sure that adaptation was indeed occurring in the LHL circuit. Finally, 45 minutes after the end of the adaptation we took a recovery measurement from RHL stimulation. This is visualized in Figure 8 below.

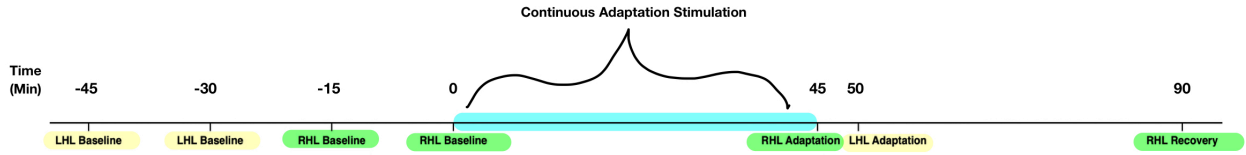

Figure 8: Cross-adaptation stimulation protocol. For this set of experiments, we attached a motor device to the bottom of each HL paw. For the first 45 minutes of the experiment, we collected 4 baseline measurements, 2 each from each HL stimulation. We then stimulated the LHL with continuous 10Hz vibrations for 1 second every 6 seconds for 45 minutes in total. After 45 minutes we stopped the continuous stimulation, let the animal rest for 2 minutes with no stimulation, and then took the RHL cross adaptation measurement by stimulating the RHL. We waited another 5 minutes before taking the LHL adaptation measurement (as a control to make sure the LHL circuit was adapting). We then took a RHL recovery measurement 45 minutes after the cessation of the continuous stimulation. In yellow are the LHL measurements where we stimulated the LHL. In green are the RHL measurements where we stimulated the RHL. In blue is the continuous adaptation phase.

2.4.4: IOS Data Analysis

This project's methods for IOS image analysis are the same as Farhoomand 2021, and are based off Chen-Bee *et al*., (2000). Each trial consists of 300 image frames which include all 3 seconds of cortical activity. An average stack of all 300 frames is made by the data collection software of all 5 trials that make up the data collection for 1 measurement. The first 100 frames (corresponding to 1 second of brain activity before stimulus onset) act as a baseline ($R_{baseline}$), and they were averaged together as one image. Then the stack of 300 frames was divided by $R_{baseline}$, and an 8-bit linear grayscale map was applied to the processed data so that any increased intrinsic signal is mapped to a grayscale value of black. In essence, this process converts the post response area of the stack into ratio values relative to pre-stimulus data

such that this processed data can now be thought of as "a mountain of activity" (as described in Chen-Bee *et al*., (2000). The x and y axis of this mountain of activity indicate cortical location, and the z-axis indicates the magnitude of the evoked signal. Once that was complete, processed frames 150 – 300 were averaged as the final image ($R_{post\_response}$). The evoked critical response starts to appear 0.5 seconds after stimulus onset, and therefore frames 150 – 300 were averaged as the final image. This process is depicted in Figure 9 below which comes from Farhoomand 2021.

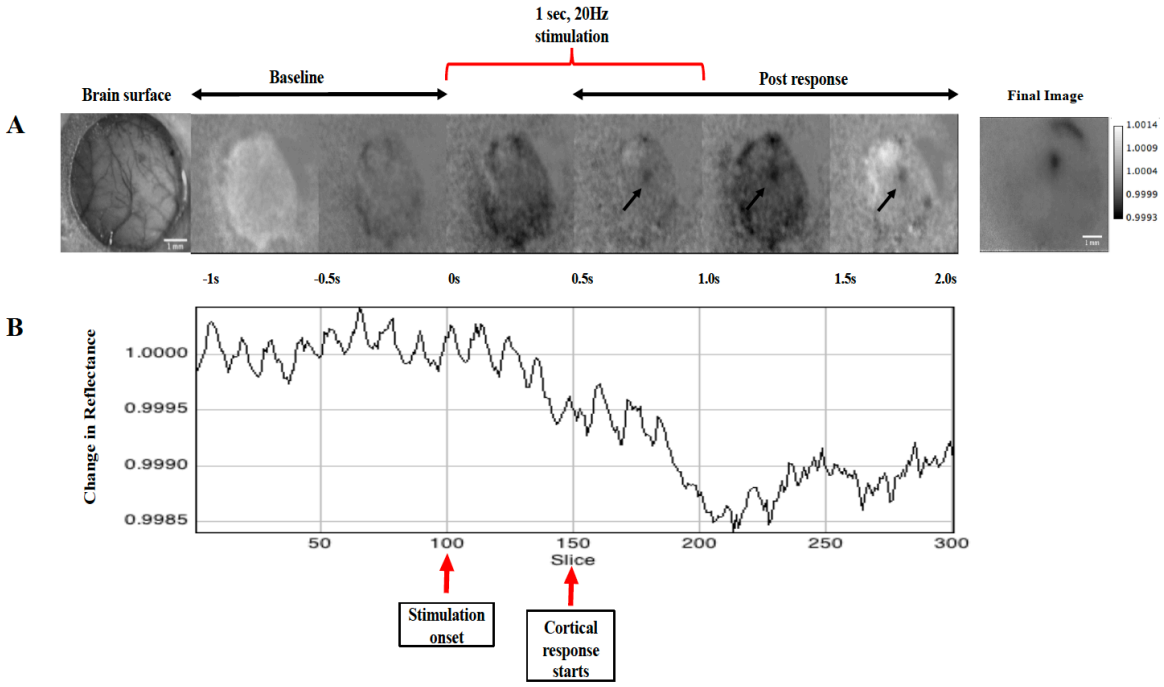

Figure 9: The first steps of IOS data analysis: collecting $R_{baseline}$ and $R_{Post\_response}$ (from Farhoomand 2021). **(A):** Cortical activity was recorded for 3 seconds in total, with 1 second being before stimulation, 1 second of stimulation, and 1 second post stimulation. The pre-stimulation second acts as a baseline. 300 frames make up the 3 seconds of brain activity data. The final image in A is collected by first averaging the first 100 frames ($R_{baseline}$). The stack of 300 frames is then divided by $R_{Baseline}$ to map changes in intrinsic signal activity to a grayscale value of black. Finally, frames 150 – 300 of this processed stack are averaged to get the final brain activity image ($R_{Post\_Response}$). **(B):** B shows evidence of the cortical response starting around slice 150.

For the final image that is used in calculating the change in reflectance, an inverted image of $R_{Post\_Response}$ with a Gaussian blur filter needs to be made. First, the first 100 frames of the processed 300 frame stack are averaged, and then a median filter of 100 pixels is applied twice. This filter baseline image is

subtracted from $R_{Post\_Response}$. This subtracted image becomes $R_{Inverted\_Post\_Response}$. A Gaussian blur of δ=2 is applied to this image to remove high frequency noise. This is the final image where measurements of change in reflectance are made. The neuronal activity in the corresponding contralateral hemisphere was thresholded to 80% of the maximal signal amplitude for that area. The area and average pixel value within that threshold region is collected. This area and average pixel value is correlated to the activity of the neurons in that area. This average value is referred to as the fractional change in reflectance throughout this paper. These processes listed within this paragraph are illustrated in Figure 10 below (adapted from Farhoomand 2021).

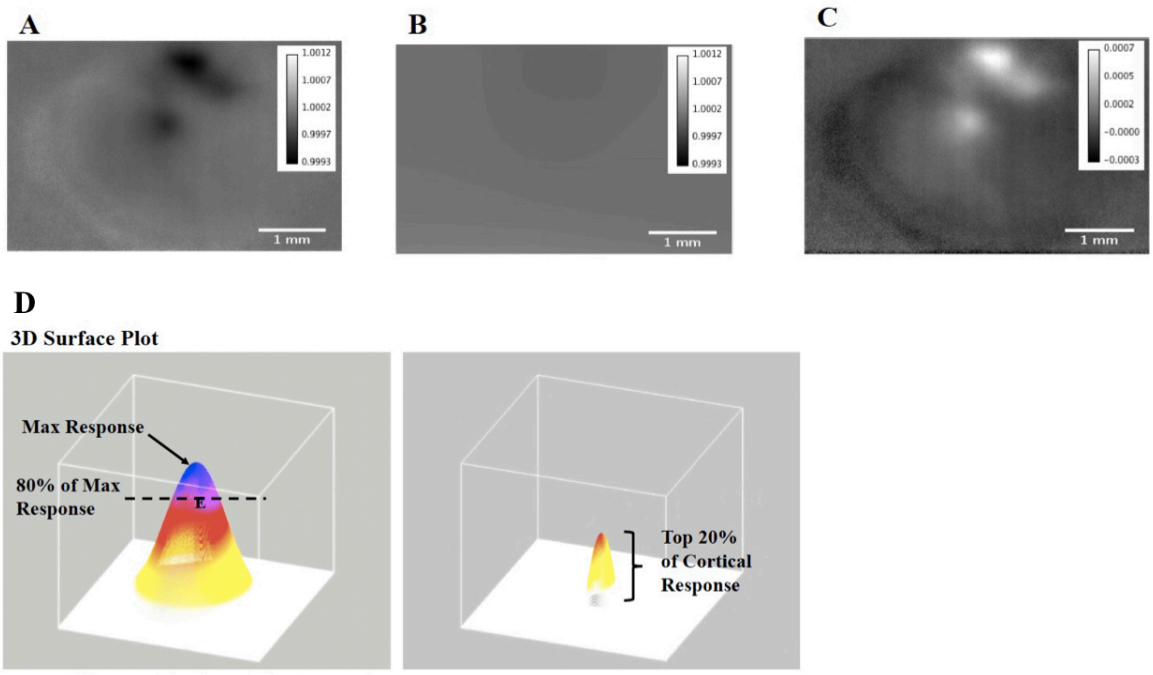

Figure 10: Measuring fractional change in reflectance. **(A):** An example of an optical image averaged from 5 trials in the barrel cortex (Farhoomand 2021) before image processing. **(B)** The average of frames 1 – 100 from the processed stack (baseline reflectance). This image has a median filter of 100 pixels applied twice. **(C):** The final image where measurement occurs. This is the result of subtracting the baseline image (B) from $R_{Post\_Response}$. A Gaussian blur of δ=2 is applied to this image to remove high frequency noise. **(D):** The response visible in (C) is thresholded to 80% of the maximum value within the response. This leaves the top 20% of the cortical response, whereby the area (in pixels) is recorded, and the average value of the pixels in that area is taken as the fractional change in reflectance.

3: Results

3.1: Comparison of motor and piezo vibratory devices within 1 animal via *in vivo* intracortical local field potential recordings

3.1.1: Comparison of CER Amplitudes

Two motor settings (Motor60mA and Motor70mA) were compared to the piezo device by stimulating the left hindlimb with a 7-stimulus test train at 10Hz and recording the resulting CER in the contralateral primary somatosensory cortex directly via *in vivo* intracortical LFP recordings. With LFP recording, the resulting CER is measured by recording an average amplitude of the CER deflection in the electrophysiological trace. Motor60mA sent a 4.28V (60mA) signal to activate the motor, and Motor70mA sent a 5V (70mA) signal to activate the motor.

The first column of Figure 11A – C displays the average CER collected from *in vivo* LFP recordings from HL stimulation via the piezo device (Figure 11A), the motor60mA settings (Figure 11B), and the motor70mA settings (Figure 11C). These average traces are each an average of 5 averages of 20 raw trace repetitions of the seven-stimulus test train. The right column of Figure 11A – C represents the average amplitude of the CER at each of the seven stimuli within the test train. Those averages for each peak were then summed to indicate a measure of the CER over 700ms (Figure 11C).

A one-way within subject ANOVA was completed on the sum of the CERs to determine whether there are statistically significant differences in the CER across the three vibratory device settings within 1 WT animal. We were able to reject the null hypothesis of no difference between the mean sums ($F = 6.78$, $df = 2, 12$, $P = 0.010$). There is a significant difference in the average mean of the sum of the CER across devices.

Probing this significant effect with post-hoc analysis (Tukey HSD) found a significant difference between the means of the piezo device and motor70mA (P = 0.0094), but no statistically significant difference between the piezo device and motor60mA settings (P = 0.072), and no statistically significant difference between both motor settings (P = 0.50). On average, the piezo device resulted in an average CER that was 0.52 ± 0.37 mV larger than the motor70mA settings. Though this difference is statistically significant, the effect size is small. In terms of the sum of the CERS, this result supports the proposition of replacing the piezo device with the motor device, especially with the motor settings at 60mA output due to there being no statistically significant difference in the sum of the CER between the 60mA motor setting and the piezo device.

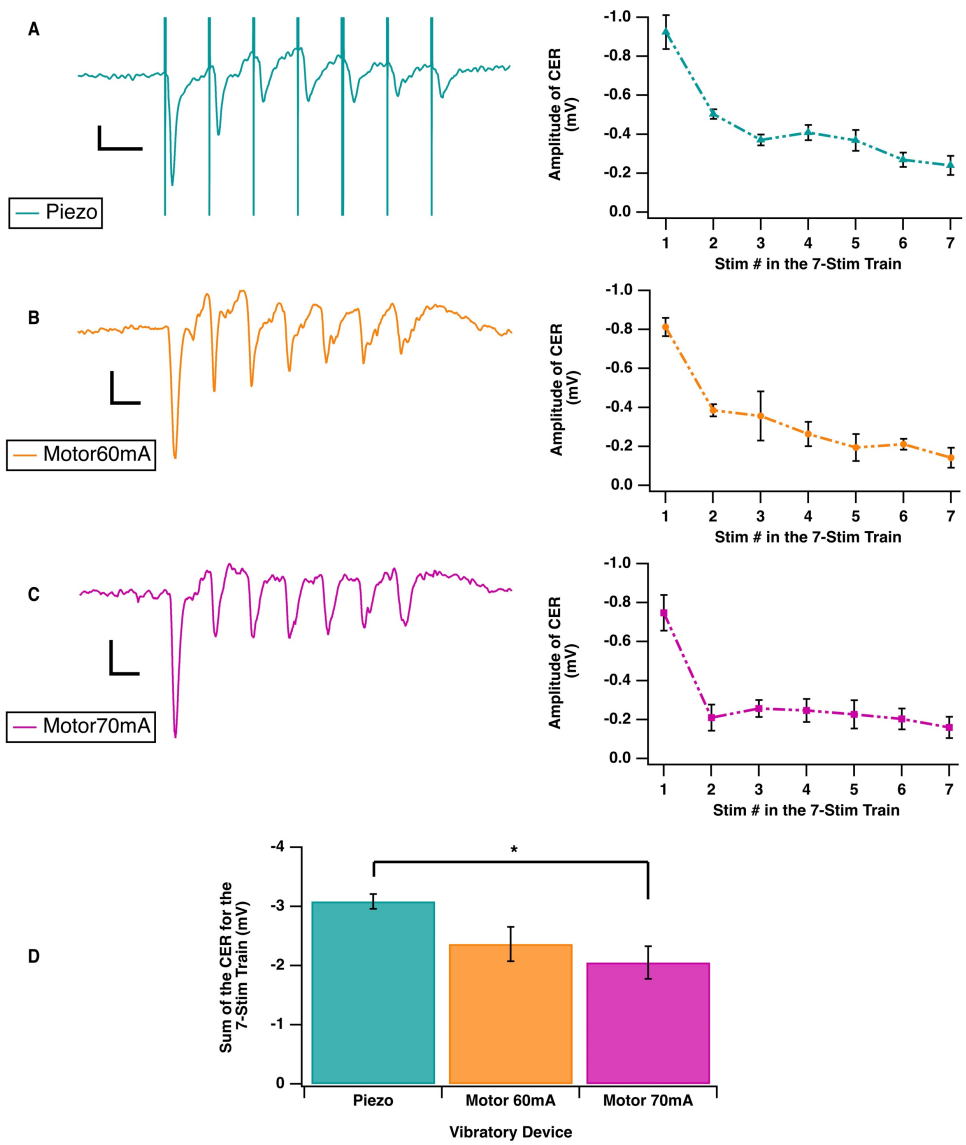

Figure 11: Summary of the amplitude of the CERS for the average of the 5 averages for each of the three vibratory devices resulting from a 7-stimulus test train where the stimuli come in at 10hz. All error bars are ± 1 standard error for the 5 averages that make up the overall average. **(A – C):** All three scale bars for the left column average traces represent 0.2mV on the y-axis and 0.1 seconds on the x-axis. The vertical lines on the average trace for the piezo device represent the stimulus artifact for each of the 7 stimuli within the test train. The right column of A – C represents the average CER amplitude resulting from each of the 7 stimulations within the test train. **(D):** A bar graph depicting the average sum of the 7 CERs within the test train for each of the three device settings. The sum of the CERs for the piezo device is -3.08 ± 0.13 mV. The sum of the CERs for the motor60mA setting is -2.24 ± 0.29 mV. The sum of the CERs for the motor70mA setting is -1.85 ± 0.27 mV. A statistically significant difference between the piezo and motor70mA settings was found ($P = 0.0094$), but no other statistically significant differences were found between the three groups.

While the sums of the CER amplitudes across devices were similar, there are obvious visual differences in the amplitudes of the CER as a function of peak number within the 7-stimulus test train across the three

vibratory device settings. This can be seen in Figure 11A-C in both the average traces (left column) and the magnitude of the CER amplitudes (right column). For example, the piezo device and the motor60mA setting show a similar graded fashion of short-term adaptation across the first 3 – 4 responses of the 7-stimulus train. Motor70mA differs in that it seems to cause a more immediate adaptation from the first to the second peak, and then remain consistent across responses 2-7 in terms of amplitude of the CERS.

To probe the potential differences in short-term adaptation within the 7-stimulus test train across the vibratory devices, we next looked at the paired pulse ratio between the 1st and 2nd CER responses. (Figure 12). Figure 12A appends the CER amplitudes as a function of stimulation number within the 7-stimulus test train from each of the devices on 1 graph to allow for easy visual comparison of the CER responses as a function of device. Figure 12b quantifies the ratio of the 2nd CER amplitude over the first CER amplitude for each device.

A one-way within subject ANOVA was completed on this paired pulse ratio to determine any significant differences across groups for this 1 WT animal. We were able to reject the null hypothesis of no significant differences across devices ($F = 6.16$, $df = 2, 12$, $P = 0.014$). There was a significant difference in paired pulse ratios. Probing this significant effect with post-hoc analysis (Tukey HSD) found a statistically significant difference in the paired pulse ratio between the piezo device and the motor70mA setting ($P = 0.012$). On average, the paired pulse ratio (P2/P1) was 0.28 ± 0.22x larger than the paired pulse ratio for the motor70mA setting. As can be seen by the size of the 95% confidence interval of the difference (±0.22x) and the error bar on the motor70mA setting, there is not as much precision for the estimate of a paired pulse ratio for motor70mA. There was more variability of paired pulse ratio in the 5 averages for motor70mA as compared to the other two vibratory devices. There were no statistically significant differences in the paired pulse ratio between the piezo and motor60mA setting ($P = 0.40$), and

between the motor60mA and the motor70mA settings (P = 0.12). These results together indicate that in general, there is a lot of initial short-term adaptation with the motor70mA settings. This could indicate that the 60mA setting might be a better replacement to the piezo as compared to the 70mA settings.

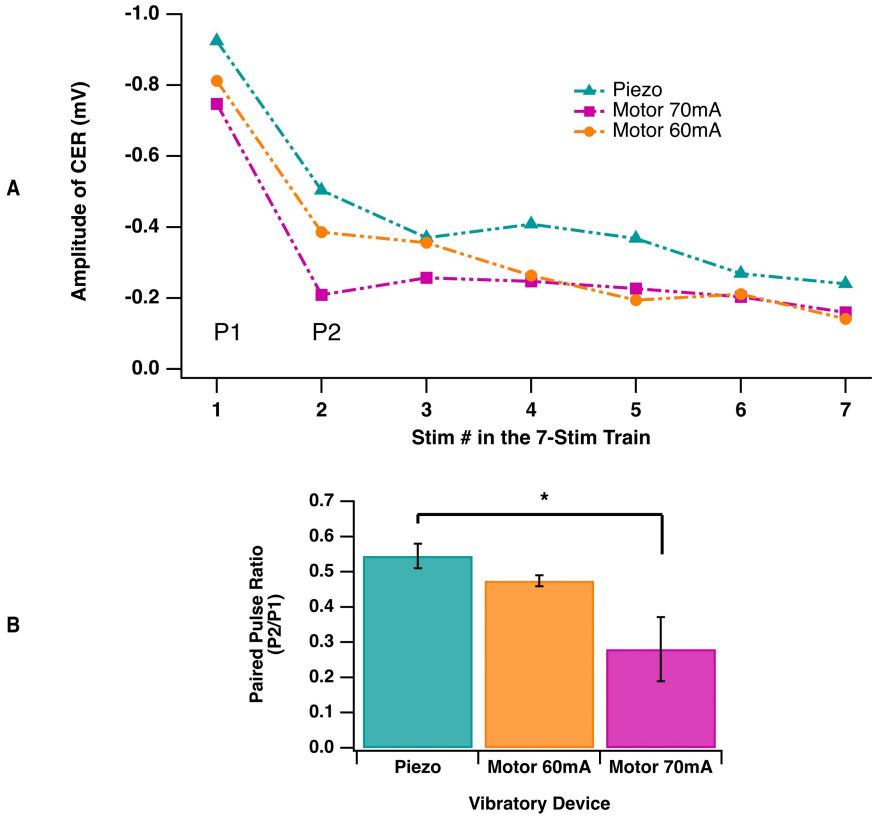

Figure 12: Paired pulse ratios for each of the three vibratory devices. **(A):** Graph depicting the magnitude of the amplitude of the CER (mV) as a function of stimulation number within the 7-stimulus test train. The P1 (Peak 1) and P2 (Peak 2) on the graph depict what was used for the calculation of the paired pulse ratio. **(B)** Bar graph representing the paired pulse ratio for each vibratory device. Error bars represent ± 1 standard error for the 5 averages that make up the overall average. The mean of the paired pulse ratio for piezo was 0.56 ± 0.034. The mean for motor60mA was 0.45 ± 0.016, and the mean for motor70mA was 0.28 ± 0.091. There was a statistically significant difference between the ratio for piezo and the motor70mA setting (P = 0.012). No other statistically significant differences were found across the groups.

3.1.2: A Difference in Timing of the CER

There are some key differences between the piezo device and the motor device. The first is that the piezo device is biphasic, and the motor device is not. The piezo also has a lot more precision in terms of how sharply it can be turned on and off. For each of the 7 stimulations within the test train, the piezo biphasic

signal is on for 1.25ms duration in the positive direction followed immediately by a 1.25ms duration in the negative direction. This is a total stimulus duration of 3ms.

In this experiment, my stimulation duration for the motor devices was 30ms. This is not biphasic and is instead 30ms in the positive direction. Another key difference between the two devices is that the piezo device leaves a stimulus artifact (seen in Figure 11A and Figure 13A), while the motor device does not. Functionally, this means that it is very easy to see for the piezo that the stimuli come in at precisely the same time for each stimulus train (you can see this because the artifacts line up perfectly in the traces). The motor device does not allow for this feature. Since the motor device doesn't leave a stimulus artifact to know when exactly the stimulus came in, we next wanted to test the timing of when the maximum deflection point occurs after the offset of the stimulus, and in the case of the motor device, this could be used as a proxy to see if the maximum deflection point was occurring around the same time in each trace. If so, then that shows that the motor can send out a consistent and reliable stimulus, indicating that the motor is also precise (which is a key feature for the purpose of averaging averages). Figure 13 below shows the results of this line of enquiry.

Figure 13A – C displays the same average of averages traces for each of the vibratory devices that was shown in Figure 11A-C. This time, rectangles have been added to the motor traces indicating the point in time where the stimulus should be occurring. We measured the change in time (on the x-axis) between the moment the stimulus turns off to the following maximum deflection point (CER) in the trace. This timing was then averaged across the 7 deflection points in the trace and further plotted in Figure 3D. Levene's Test was employed on this data set to test whether the variation in the timing between stimulus offset and max deflection of the CER was equal across the groups. We were unable to reject the null hypothesis of equal variance between groups ($F = 1.30$, $df = 20, 84$, $P = 0.20$). This means that there was

no statistically significant difference in the variance of timing across each of the three vibratory devices. In summary, this gives evidence that the motor devices were statistically equally accurate in terms of precision of the stimulation for this animal, because if they weren't, we would have seen more variation in the timing between the theoretical stimulus offset and the peak deflection of the CER. This allows us to conclude that the motor device can be a reliable replacement to the piezo device.

Along with equal variance in the timing between stimulus offset and peak deflection, Figure 13D shows a major difference across the devices. This is in terms of the timing itself. A one-way within subject ANOVA was completed on the data to determine whether there are statistically significant differences in the timing in seconds between the stimulus offset and the peak negative deflection of the CER. We were able to reject the null hypothesis of no difference in this timing ($F = 631.24$, $df = 2, 102$, $P = 2.2 \times 10^{-16}$). Further post-hoc analysis confirmed that each group was statistically significant from the other. For motor70mA the average timing between stimulus offset and the position of maximum deflection of the CER was 67.27 ± 1.51ms. The timing for motor60mA was 63.51 ± 0.61ms, and the timing for the piezo device was 20.26 ± 0.78ms. The piezo device resulted in a CER max deflection arriving 43.25 ± 3.5ms faster than the motor60mA setting ($P < 0.0001$) and 47.02 ± 3.49ms faster than the motor70mA setting ($P < 0.0001$). The motor 60mA setting was 3.77 ± 3.50ms faster than the motor70mA setting. This indicates that the motor and piezo devices do differ in terms of timing. Each device is reliably consistent, but the timing between stimulus offset and the position of maximum deflection of the CER is different.

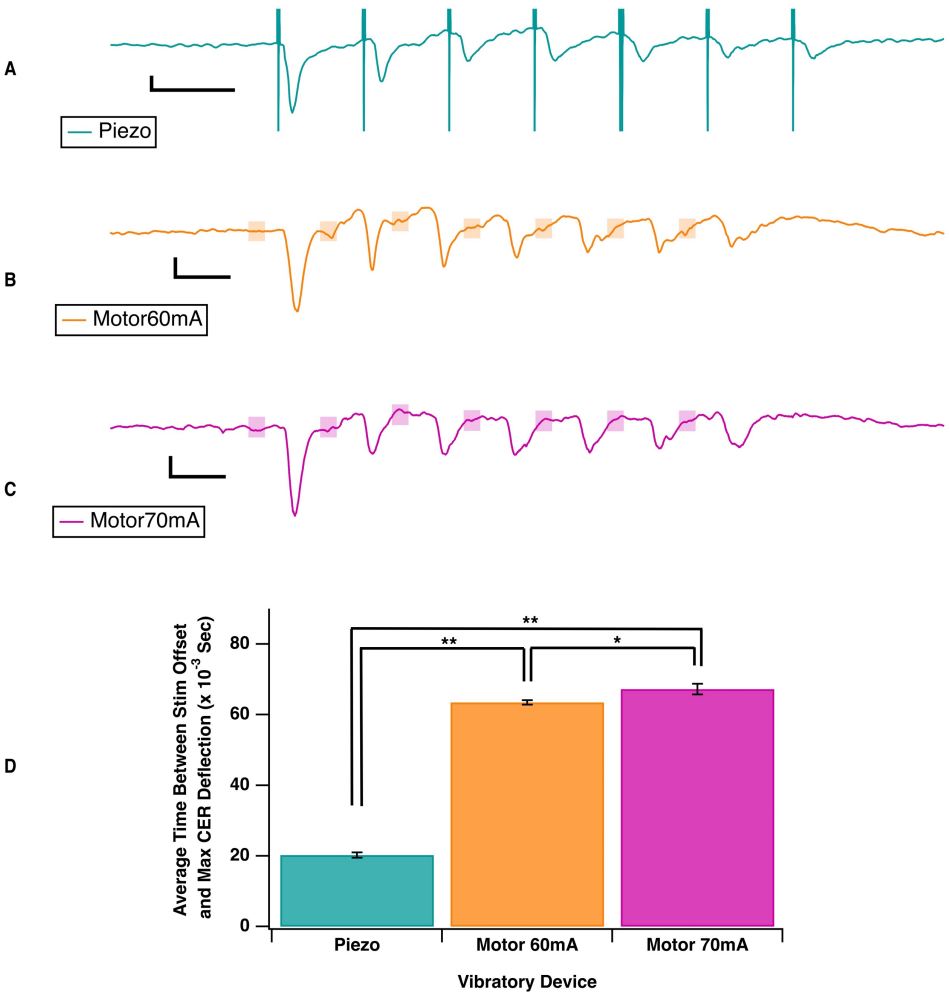

Figure 13: Timing between the stimulus offset and the position (s) of the maximum deflection of the CER. **(A – C):** The average trace of the 5 averages for each of the vibratory devices. The scale bars for all three indicate 0.2mV on the y-axis and 0.1s on the x-axis. The theoretical stimulus location for the motor devices is depicted by the lightly colored rectangles. The stimulus onset is the left side of each rectangle, and the stimulus offset is the right side of each rectangle. The change in x (as a measure of time in s) was measured from the offset of the stimulus to the resulting maximum negative deflection. **(D):** Bar graph depicting the average time between the stimulus offset and the resulting maximum negative deflection (s) for each of the vibratory devices. Levene's test showed that there was equal variance in terms of the timing for each of the vibratory devices ($P = 0.20$). A one-way ANOVA showed statistically significant differences in the timing across the three groups ($P = 2.2 \times 10^{-16}$). The piezo device resulted in a CER max deflection arriving 43.25 ± 3.5ms faster than the motor60mA setting ($P < 0.0001$) and 47.02 ± 3.49ms faster than the motor70mA setting ($P < 0.0001$). The motor 60mA setting was 3.77 ± 3.50ms faster than the motor70mA setting.

3.2: Comparison of the Contralateral and Ipsilateral Responses to Motor Stimulation with IOS Imaging

Now we move to our analysis of IOS imaging. With IOS imaging, the resulting CER is measured by calculating the fractional change in reflectance of the deoxygenated blood. Our use of an 8mm glass

coverslip instead of a 5mm glass coverslip has allowed for the investigation of the resulting CERs in both the contralateral and ipsilateral hemispheres at the same time from vibratory stimulation at one paw. The data from Figure 14 below are the result of stimulating the left hindlimb with the motor70mA setting at 10Hz 1 second vibrations. 5 rounds of 1 second 10Hz stimulations were delivered with a 14 second interval between each one, and the average response for the CER in each hemisphere was calculated from those 5. The data in Figure 14 is the average of 3 animals.

Figure 14A shows the average fractional change in reflectance as a function of the side of the brain across three different animals. A paired two-sample t-test allowed us to reject the null hypothesis of no difference between the average fractional change in reflectance as a function of brain hemisphere (t = 13.42, df = 2, P = 0.0056). There is a statistically significant difference in the fractional change in reflectance across the two groups. On average, the mean change in reflectance for the contralateral hemisphere is $4.11 \times 10^{-4} \pm 1.32 \times 10^{-4}$ times larger than the change in reflectance for the ipsilateral hemisphere.

Figure 4B shows the average pixel size of the top 80% of the CER response for each hemisphere. With a paired two-sample t-test we were unable to reject the null hypothesis of there being no difference in the mean area of the responses (in pixels) across the hemispheres (t = -2.58, df = 2, P = 0.12). There is no statistically significant difference between the contralateral and ipsilateral hemispheres in terms of the average area of the top 80% of the CER response.

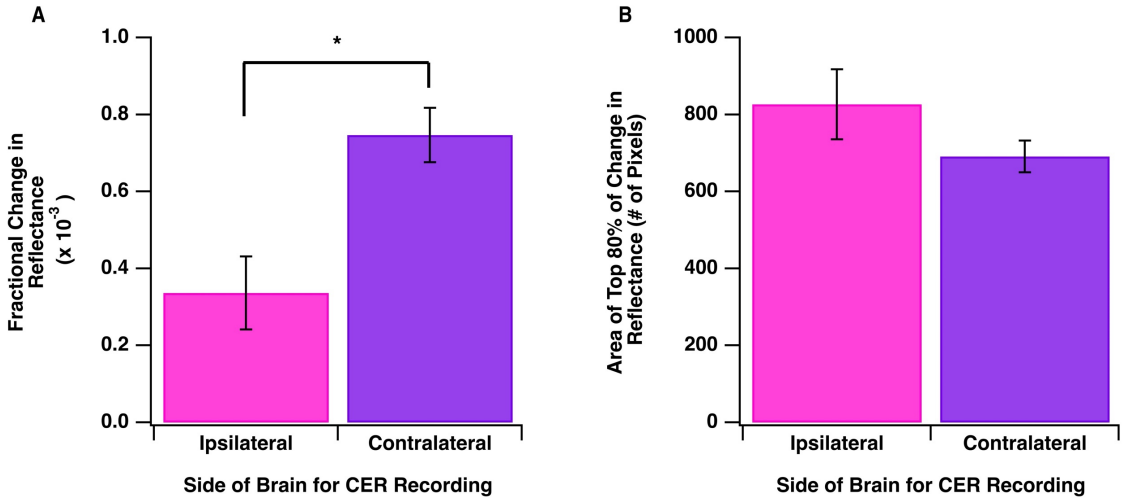

Figure 14: Comparison of the ipsilateral and contralateral hemispheres in terms of the fractional change in reflectance measurements and the area (in pixels) of the top 80% of the CER responses. **(A):** Bar graph depicting the average fractional change in reflectance as a function of the CER being in either the ipsilateral (pink) or contralateral (purple) hemisphere (N = 3). The average for the ipsilateral side is 3.36 x 10^{-4} ± 9.49 x 10^{-5}. The average for the contralateral side is 7.47 x 10^{-4} ± 7.07 x 10^{-5}. There is a statistically significant difference between the groups (P = 0.0056). **(B):** Bar graph depicting the average area (# of pixels) of the top 80% of the CER response as a function of hemisphere (N = 3). The average for the ipsilateral side is 826.33 ± 90.84 pixels. The average for the contralateral side is 691.33 ± 40.96. This difference in average area is not statistically significant (P = 0.12).

3.3: Evidence for Adaptation with IOS Imaging

The results of the adaptation experiment are illustrated below in Figure 15. A baseline response was established in the contralateral hemisphere (in these experiments the right hemisphere) by stimulating the left hindlimb with the motor70mA setting at 10Hz 1 second vibrations. 5 rounds of 1 second 10Hz stimulations were delivered with a 14 second interval between each one, and the average response for the CER in each hemisphere was calculated from those 5. This constitutes 1 baseline response. This was repeated 15 minutes later for a second baseline response. These two baseline measurements were then averaged for the overall baseline response for that animal for the experiment. A total of 3 animals are averaged in this adaptation experiment, and the results are plotted in Figure 15A. After the second baseline response, we ran a continuous stimulation paradigm on the left hindlimb (the adaptation phase) where we stimulated the hindlimb at 10Hz for 1 second every 6 seconds for 45 minutes in total (shown as the grey rectangles in Figure 15). For the adaptation measurement, we stopped the repetitive stimulation,

waited for 2 minutes, and then recorded the CER again in the contralateral hemisphere with the same stimulation paradigm as what was used for the baseline measurement. This was repeated 45 minutes later for the recovery measurement. The recovery measurement was used as a control measure to make sure that the adaptation response came back towards baseline.

To ensure that the baseline measurements were not statistically different from each other (N = 3), a paired t-test was conducted, and we were unable to reject the null hypothesis of no difference between the two baseline measurements (t = -0.56, df = 2, P = 0.63). The two baseline measurements were not statistically different from each other, and they are therefore a reliable baseline to use. Next, a one-way repeated measures ANOVA was completed to determine if there were significant differences between the baseline measurement, the adaptation measurement, and the recovery measurement. We were able to reject the null hypothesis of no difference between these groups (F = 13.41, df = 2, 6, P = 0.0061). Probing this with post hoc analysis (Tukey HSD) found that the fractional change in reflectance for the adaptation measurement was smaller than the baseline measurement by $5.95 \times 10^{-4} \pm 3.74 \times 10^{-4}$ (P = 0.0067), and smaller than the recovery measurement by $4.83 \times 10^{-4} \pm 3.74 \times 10^{-4}$ (P = 0.018). There was no statistically significant difference between the baseline measurement and the recovery measurement (P =0.65).

Figure 15B normalizes this data set by plotting each measurement from Figure 15A as a ratio out of the baseline measurement. The adaptation measurement was 31.5 ± 18.3% of the baseline measurement. The recovery measurement 45 minutes after the end of the adaptation phase was 86.1 ± 9.2% of the baseline measurement.

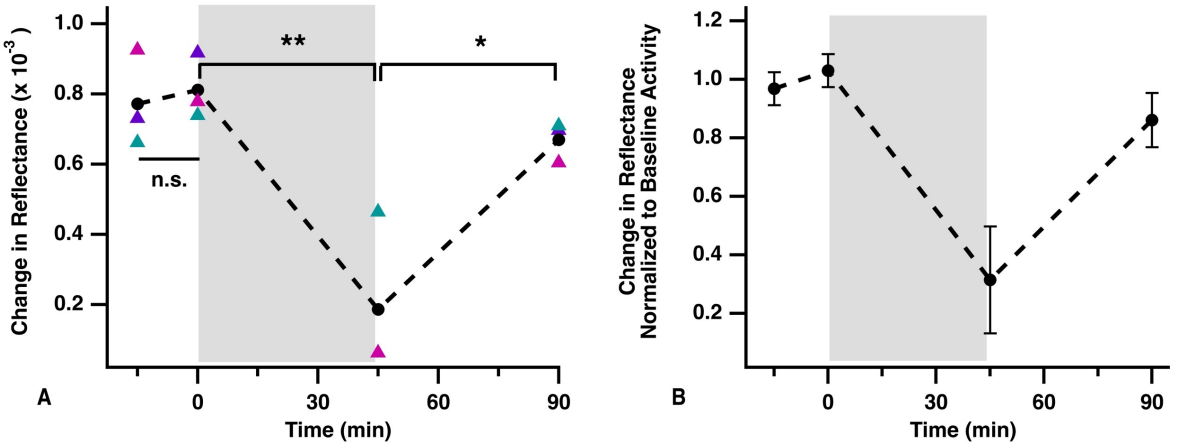

Figure 15: Line graphs depicting the adaptation experiment. The grey bar on each graph represents the 45-minute period of repetitive stimulation that constitutes the adaptation phase. **(A):** Line graph plotting the average change in reflectance as a function of time (min) for 2 baseline measurements (-15 and 0 mins), 1 adaptation measurement (45 mins), and one recovery measurement (90 mins) (N = 3). The 'n.s.' under the baseline measurements indicates no significant difference between the two baseline measurements ($P = 0.63$). The colored data points represent the raw data for the 3 WT animals. The adaptation average is significantly smaller than both the baseline measurement ($P = 0.0067$) and the recovery measurement ($P = 0.018$). There was no significant difference between the baseline measurement and the recovery measurement ($P = 0.65$). **(B):** The same data as (A) but normalized to the baseline response. The error bars indicate ± 1 standard error. The adaptation measurement is 31.5 ± 18.3% of the baseline measurement. The recovery measurement 45 minutes after the end of the adaptation phase was 86.1 ± 9.2% of the baseline measurement.

3.4: Evidence for Cross Adaptation with IOS Imaging

The results of the cross-adaptation experiment are illustrated below in Figure 16. We wanted to know if there was evidence for cross adaptation, meaning that does causing adaptation in the circuit from left hindlimb to the contralateral hemisphere (right hemisphere) also cause adaptation in the opposite circuit when you stimulate the right hindlimb and record from the contralateral hemisphere (left hemisphere). We therefore needed two motor devices, one attached to each hindlimb. The motor70mA settings were used for this. One of these motors could be stimulated at one time to allow us to record from the contralateral hemisphere.

Due to stimulating and recording from both circuits, a baseline response needed to be established for the contralateral hemisphere for both hindlimbs. This was done by first stimulating the left hindlimb, while recording the contralateral response in the right hemisphere, then waiting 15 minutes and

stimulating the right hindlimb and recording the contralateral response in the left hemisphere. This process was repeated so that there were two baseline measurements for both hindlimb stimulations. A total of 2 animals are averaged in this adaptation experiment, and the results are plotted in Figure 16A. As can be noted from the graph, the measurements for the left hindlimb stimulation are not included on the graph, because the right hindlimb measurements are what we used for cross-adaptation. The left hindlimb stimulation was simply a control to ensure that adaptation in the left hindlimb circuit was adapting.

After the second baseline response on the right hindlimb stimulation, we ran a continuous stimulation paradigm on the left hindlimb (the adaptation phase) where we stimulated the left hindlimb at 10Hz for 1 second every 6 seconds for 45 minutes in total (shown as the grey rectangles in Figure 6). For the cross-adaptation measurement, we stopped the repetitive stimulation, waited for 2 minutes, and then stimulated the opposite paw (right paw) to record the contralateral CER in the contralateral hemisphere (left hemisphere). We then waited a further two minutes and stimulated the left hind paw again to ensure that adaptation was indeed occurring (as was to be expected from the results in Figure 15). We then waited a further 45 minutes before stimulating the right hindlimb again for the recovery measurement in the contralateral hemisphere. Like with the adaptation experiment, the recovery measurement was used as a control measure to make sure that the adaptation response came back towards baseline.

To ensure that the baseline measurements were not statistically different from each other (N = 2), a paired t-test was conducted, and we did not reject the null hypothesis of no difference between the two baseline measurements (t = -0.23, df = 1, P = 0.86). The two baseline measurements were not statistically different from each other, and they are therefore a reliable baseline to use. Next, a one-way

repeated measures ANOVA was completed to determine if there were significant differences between the baseline measurement, the adaptation measurement, and the recovery measurement. We failed to reject the null hypothesis of no difference between these groups (F = 0.33, df = 2, 3, *P* = 0.74). As can be seen from Figure 16A, there is still evidence for a decrease in the change of reflectance for the adaptation measurement, but this test revealed that this difference is not statistically significant. It is likely that this is simply not yet statistically significant, as the pattern is there, but the N is very small (N = 2), and there is a large difference in the magnitude of the change in reflectance measurements across the two animals. More animals are likely needed to uncover an effect here.

Figure 16B normalizes this data set by plotting each measurement from Figure 16A as a ratio out of the baseline measurement. The adaptation measurement was 60.4 ± 10.9% of the baseline measurement. The recovery measurement 45 minutes after the end of the adaptation phase was 109 ± 13.3% of the baseline measurement.

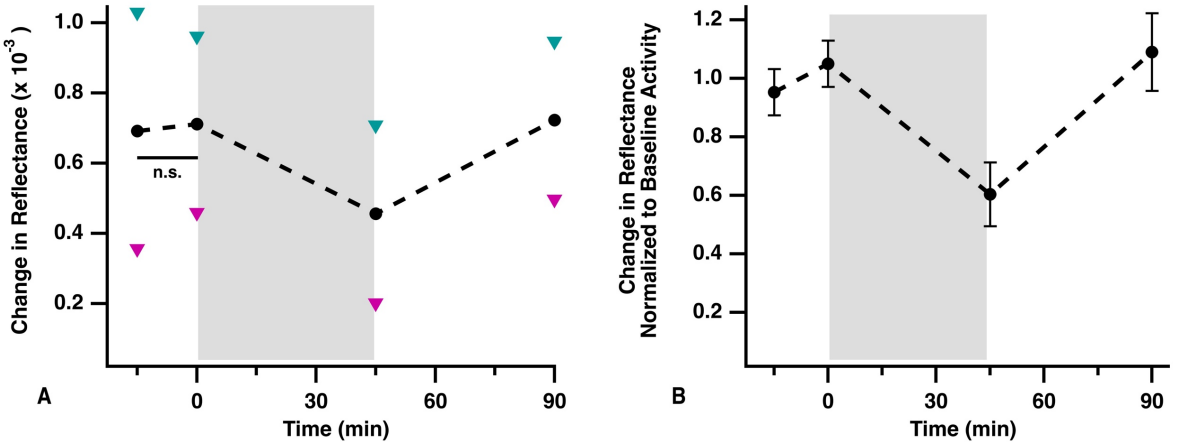

Figure 16: Line graphs depicting the cross-adaptation experiment. The grey bar on each graph represents the 45-minute period of repetitive stimulation in the left hindlimb circuit that constitutes the adaptation phase. **(A):** Line graph plotting the average change in reflectance as a function of time (min) for 2 baseline measurements (-15 and 0 mins), 1 adaptation measurement (45 mins), and one recovery measurement (90 mins) for the right hindlimb circuit (N = 2). The 'n.s.' under the baseline measurements indicates no significant difference between the two baseline measurements (*P* = 0.86). The colored data points represent the raw data for the 2 WT animals. We found no significant difference between groups (F = 0.33, df = 2, 3, *P* = 0.74). The difference between the adaptation measurement and the baseline measurement that is visible on the graph is not yet statistically significant, and this is likely due to sample size. **(B):** The same data as

(A) but normalized to the baseline response. The error bars indicate ± 1 standard error. The cross-adaptation measurement is 60.4 ± 10.9% of the baseline measurement. The recovery measurement 45 minutes after the end of the adaptation phase was 109 ± 13.3% of the baseline measurement.

4: Discussion

This goal of this project was to establish a new protocol to further probe the STA and PSA that was found in Farhoomand (2021). To do so, we needed to test the ability to use a larger glass coverslip (8mm rather than 5mm) for the cranial window so that we could record from both HL primary somatosensory cortices simultaneously. We were successful in this endeavour, as is seen in Figure 3 (under the IOS surface imaging section within LFP electrophysiology methods). In this image you can clearly see the response in the contralateral right hemisphere and the ipsilateral left hemisphere.

To satisfy the overall goal of establishing a new protocol, this project sought to answer three main questions: (1) Can we replace the piezo device with the motor device, (2) Do we see the same adaptation phenomenon as was found in Farhoomand (2021), and (3) Now that we can simultaneously record from both hemispheres, is there evidence for cross adaptation in the opposite HL to primary somatosensory cortex cortical circuit. The remainder of the discussion will focus on the answer to these questions, one at a time.

4.1: Can we replace the piezo device with a motor device?

Through electrophysiological data, we found that the only significant difference between the piezo and motor device was the fact that the max deflection points of the peak change in the CER occurred an average of 45ms sooner after stimulus offset with the piezo device as compared to the motor device. This isn't super surprising when you consider that these are two different vibratory devices that send out very different types of vibrations. The piezo is sharp and intense, while the motor device is more drawn

out, less intense, and shakes the paw a bit more than the piezo does. This shake of the paw may be activating more of the proprioceptive fibers within the sensory circuit as compared to the piezo. The shaking and lighter vibration of the motor device may also activate less of the deeper mechanoreceptors of the skin than the piezo. All these factors could likely contribute to this difference in timing of the CER.

Another possibility could be that the motor device is not sending out the stimulation right when the computer software tells it to. This is one downside of the motor device not leaving an artifact within the LFP trace. You don't know for sure if it is activating the motor when it should be. The consistency of the data combined with the consideration of different fibers within the sensory pathway having the ability to send information at different speeds suggests that the motor is very likely sending the vibration when it should be and this difference is more likely to be due to the stimuli sending different vibrations, and therefore causing their own unique neural signature in terms of timing.

In terms of similarities across devices, the sum of the CER and the peak 2 over peak 1 ratio of the motor60Ma device setting was not significantly different than the piezo device, and this is evidence that the same pattern of STA that was found in Farhoomand (2021) and replicated here for the piezo device is also occurring with the motor device within this 1 animal. Further animals should be tested to confirm whether this pattern remains for the motor device, but for now this is sufficient evidence for us to be satisfied that the motor device can reliably replace the piezo device.

4.2: Is there evidence for the same adaptation phenomenon that was found in Farhoomand (2021)?

Our results from figure 15 show that after the adaptation phase, the CER was reduced by 31.5 ± 18.3%. As a comparison, the age matched WT mice from Farhoomand (2021) had a reduction of 35.17 ± 5.4% after the adaptation phase and the RTT mice of that age cohort had a reduction of 43.38 ± 6.8%. These

are very similar, and evidence that the motor does indeed produce an STA phenomenon like the piezo does.

A major difference in our data set is the fact that our recovery measurement at 45 minutes after continuous stimulation came back up to 86.1 ± 9.2% of the baseline measurement and was therefore statistically different from the adaptation measurement. This was not the case in the WT mice in Farhoomand (2021) and is not exactly like the RTT mice in terms of timing of recovery. There are a couple reasons why this could be the case.

The first reason is that with the continuous adaptation protocol we set up for this project, we attempted the repetitive stimulation protocol with 10hz 1 second stimulations rather than 100hz from Farhoomand. The reason for the 10hz stimulation rather than 100hz stimulation for the repetitive paradigm was that the 100hz made the whole leg shake quite a bit. We decided to drop it down to 10Hz because that frequency shook the paw and leg much less. Maybe this 10hz stimulation was enough to cause the STA but not the consolidated and persistent form of adaptation (PA) found in Farhoomand. We will want to repeat these experiments with higher frequency to see if that is the case. To do so, we may have to adjust the duration of each stimulation within the 1 second stimulation during the IOS sessions. In summary, we have good evidence for STA with the motor device, but not yet with PA.

Another reason for this difference in timing of the recovery could be the difference in timing of the adaptation phase. We adapted for 45 minutes instead of 1 hour because; (1) the adaptation phase of the last 15 minutes did not cause significant changes to the resulting CER, and (2) we hoped to decrease the length of time under anesthesia for the experiment because we intend to add a repeated measures element to our design and would prefer to have each experiment as short as possible due to repeating it

within animals. Maybe the extra 15 minutes causes a change to the timing of the recovery from PA. This is something that could be tested for by comparing an adaptation phase of 45 minutes to an adaptation phase of 1 hour. In summary though, this is all supportive evidence for adaptation being present with the motor device.

4.3: Is There Evidence for Cross-Adaptation?

As can be seen in Figure 17, there was a visual reduction in the fractional change in reflectance after the adaptation phase of the opposite circuit, but this reduction was not statistically significant. This was very likely not statistically significant due to the small sample size (only N = 2) and the variability in the magnitude of the responses between the two animals. This means that there is evidence for cross-adaptation, but more animals will need to be tested to determine this. It will also be useful to add another protocol that uses a 100Hz repetitive stimulation to see if there are differences as a function of the strength of the stimulation.

4.4: Limitations and Future Directions

The main limitation with all these experiments is the small sample size. For the LFP experiment there was only a sample of 1, and the comparisons are therefore all within 1 animal. While the information is useful for determining the consistency of the motor device within 1 animal, the sample size will need to be increased to ensure that the consistency of the motor device remains across animals too.

Another limitation comes in with IOS when comparing the ipsilateral and contralateral hemispheres. As can be seen from Figure 14, the fractional change in reflectance for the ipsilateral hemisphere was only $3.36 \times 10^{-4} \pm 9.49 \times 10^{-5}$. That is a very small fractional change. Due to this, we were not able to determine if the ipsilateral side adapts during the adaptation experiment (which we had hoped

to do). The reason we couldn't determine if the ipsilateral side adapts is the fact that the signal became lost in the noise after the adaptation phase. That is promising news for there being evidence of cross-adaptation because the response was always there at baseline and visibly disappeared after adaptation, but this change was not quantifiable. An alternative solution may be the method of using a voltage-sensitive dye (VSD) with optical signal imaging rather than relying on blood changes like in IOS. VSD is another very common optical imaging method for measuring neocortical activity across animal species (Grinvald *et al* 2016). There has also been success with simultaneous IOS and VSD recordings in rats (Ma *et al,* 2013). The VSD method or simultaneous VSD and IOS methodology could help us better measure the ipsilateral response, and more thoroughly quantify and further describe all other responses too.

A further avenue of exploration for us is the addition of a treatment protocol with Mirtazapine (MTZ). MTZ is a widely used noradrenergic and specific-serotonergic antidepressant that has a solid safety profile and has been shown to normalize PV levels in the primary motor cortex and preserve motor learning from deteriorating in RTT mice (Gutierrez *et al* 2020). It has also been shown to rescue cortical atrophy and respiratory deficits in RTT mice (Bittolo *et al* 2016). Our non-invasive optical imaging protocols make this project viable for adding a treatment of MTZ as a repeated measure to see if the lack of PA consolidation in RTT mice can be reverted.

4.5: Conclusion

In summary, the goal of this project was to establish a new protocol that includes a larger cranial window and a new vibratory device to further probe sensory adaptation in a mouse model of RTT. We have successfully shown that the motor device sends out a consistent and reliable stimulation, and that there is evidence for adaptation and cross adaptation (though the evidence of cross-adaptation was not yet statistically significant). The continuation of this work will test a continuous stimulation paradigm of

100hz with the motor, as well as different stimulus durations. We plan to consider a VSD method to get a better signal to noise ratio for quantifying the ipsilateral response and its adaptation. We also plan to add a treatment protocol with MTZ in the hopes that MTZ can rescue the sensory deficits in the lack of consolidation found in Farhoomand (2021). The purpose of this line of enquiry is to better understand the loss of MeCP2 functioning in neuronal circuit and sensory processing. We hope that this will continue to add useful data and information towards a better understanding of RTT, better treatment for RTT, and therefore more enjoyable lives for the patients and their loved ones who suffer from RTT.

References

Arcelli, P., Frassoni, C., Regondi, M. C., De Biasi, S., & Spreafico, R. (1997). GABAergic neurons in mammalian thalamus: a marker of thalamic complexity? *Brain Research Bulletin*, *42*(1), 27–37. https://doi.org/10.1016/s0361-9230(96)00107-4

Bellini, E., Pavesi, G., Barbiero, I., Bergo, A., Chandola, C., Nawaz, M. S., Rusconi, L., Stefanelli, G., Strollo, M., Valente, M. M., Kilstrup-Nielsen, C., & Landsberger, N. (2014). MeCP2 post-translational modifications: a mechanism to control its involvement in synaptic plasticity and homeostasis? *Frontiers in Cellular Neuroscience*, *8*. https://www.frontiersin.org/article/10.3389/fncel.2014.00236

Bienvenu, T., Carrié, A., de Roux, N., Vinet, M. C., Jonveaux, P., Couvert, P., Villard, L., Arzimanoglou, A., Beldjord, C., Fontes, M., Tardieu, M., & Chelly, J. (2000). MECP2 mutations account for most cases of typical forms of Rett syndrome. *Human Molecular Genetics*, *9*(9), 1377–1384. https://doi.org/10.1093/hmg/9.9.1377

Bittolo, T., Raminelli, C. A., Deiana, C., Baj, G., Vaghi, V., Ferrazzo, S., Bernareggi, A., & Tongiorgi, E. (2016). Pharmacological treatment with mirtazapine rescues cortical atrophy and respiratory deficits in MeCP2 null mice. *Scientific Reports*, *6*, 19796. https://doi.org/10.1038/srep19796

Chen-Bee, C. H., Polley, D. B., Brett-Green, B., Prakash, N., Kwon, M. C., & Frostig, R. D. (2000). Visualizing and quantifying evoked cortical activity assessed with intrinsic signal imaging. *Journal of Neuroscience Methods*, *97*(2), 157–173. https://doi.org/10.1016/s0165-0270(00)00180-1

Clemente-Perez, A., Makinson, S. R., Higashikubo, B., Brovarney, S., Cho, F. S., Urry, A., Holden, S. S., Wimer, M., Dávid, C., Fenno, L. E., Acsády, L., Deisseroth, K., & Paz, J. T. (2017). Distinct Thalamic Reticular Cell Types Differentially Modulate Normal and Pathological Cortical Rhythms. *Cell Reports*, *19*(10), 2130–2142. https://doi.org/10.1016/j.celrep.2017.05.044

Farhoomand, F. (2021). *Sensory-evoked activity in somatosensory cortex as a model to probe cortical plasticity in a mouse model of Rett syndrome* [Thesis]. https://dspace.library.uvic.ca/handle/1828/13330

Ferezou, I., Haiss, F., Gentet, L. J., Aronoff, R., Weber, B., & Petersen, C. C. H. (2007). Spatiotemporal dynamics of cortical sensorimotor integration in behaving mice. *Neuron*, *56*(5), 907–923. https://doi.org/10.1016/j.neuron.2007.10.007

Flores Gutiérrez, J., De Felice, C., Natali, G., Leoncini, S., Signorini, C., Hayek, J., & Tongiorgi, E. (2020). Protective role of mirtazapine in adult female Mecp2+/− mice and patients with Rett syndrome. *Journal of Neurodevelopmental Disorders*, *12*(1), 26. https://doi.org/10.1186/s11689-020-09328-z

Fu, C., Armstrong, D., Marsh, E., Lieberman, D., Motil, K., Witt, R., Standridge, S., Lane, J., Dinkel, T., Jones, M., Hale, K., Suter, B., Glaze, D., Neul, J., Percy, A., & Benke, T. (2020). Multisystem comorbidities in classic Rett syndrome: a scoping review. *BMJ Paediatrics Open*, *4*(1), e000731. https://doi.org/10.1136/bmjpo-2020-000731

Girard, M., Couvert, P., Carrié, A., Tardieu, M., Chelly, J., Beldjord, C., & Bienvenu, T. (2001). Parental origin of de novo MECP2 mutations in Rett syndrome. *European Journal of Human Genetics: EJHG*, *9*(3), 231–236. https://doi.org/10.1038/sj.ejhg.5200618

Grinvald, A., Omer, D. B., Sharon, D., Vanzetta, I., & Hildesheim, R. (2016). Voltage-Sensitive Dye Imaging of Neocortical Activity. *Cold Spring Harbor Protocols*, *2016*(1), pdb.top089367. https://doi.org/10.1101/pdb.top089367

Groh, A., Bokor, H., Mease, R. A., Plattner, V. M., Hangya, B., Stroh, A., Deschenes, M., & Acsády, L. (2014). Convergence of cortical and sensory driver inputs on single thalamocortical cells. *Cerebral Cortex (New York, N.Y.: 1991)*, *24*(12), 3167–3179. https://doi.org/10.1093/cercor/bht173

Hlushchuk, Y., & Hari, R. (2006). Transient Suppression of Ipsilateral Primary Somatosensory Cortex during Tactile Finger Stimulation. *The Journal of Neuroscience*, *26*(21), 5819–5824. https://doi.org/10.1523/JNEUROSCI.5536-05.2006

Houser, C. R., Vaughn, J. E., Barber, R. P., & Roberts, E. (1980). GABA neurons are the major cell type of the nucleus reticularis thalami. *Brain Research*, *200*(2), 341–354. https://doi.org/10.1016/0006-8993(80)90925-7

Iadecola, C. (2017). The Neurovascular Unit Coming of Age: A Journey through Neurovascular Coupling in Health and Disease. *Neuron*, *96*(1), 17–42. https://doi.org/10.1016/j.neuron.2017.07.030

Ito-Ishida, A., Ure, K., Chen, H., Swann, J. W., & Zoghbi, H. Y. (2015). Loss of MeCP2 in Parvalbumin-and Somatostatin-Expressing Neurons in Mice Leads to Distinct Rett Syndrome-like Phenotypes. *Neuron*, *88*(4), 651–658. https://doi.org/10.1016/j.neuron.2015.10.029

Laurvick, C. L., Klerk, N. de, Bower, C., Christodoulou, J., Ravine, D., Ellaway, C., Williamson, S., & Leonard, H. (2006). Rett syndrome in Australia: A review of the epidemiology. *The Journal of Pediatrics*, *148*(3), 347–352. https://doi.org/10.1016/j.jpeds.2005.10.037

Li, W. (2022). Excitation and Inhibition Imbalance in Rett Syndrome. *Frontiers in Neuroscience*, *16*. https://www.frontiersin.org/article/10.3389/fnins.2022.825063

Lipton, M. L., Fu, K.-M. G., Branch, C. A., & Schroeder, C. E. (2006). Ipsilateral hand input to area 3b revealed by converging hemodynamic and electrophysiological analyses in macaque monkeys. *The Journal of Neuroscience: The Official Journal of the Society for Neuroscience*, *26*(1), 180–185. https://doi.org/10.1523/JNEUROSCI.1073-05.2006

Lotan, M., & Ben-Zeev, B. (2006). Rett Syndrome. A Review with Emphasis on Clinical Characteristics and Intervention. *The Scientific World Journal*, *6*, 1517–1541. https://doi.org/10.1100/tsw.2006.249

Ma, H., Zhao, M., & Schwartz, T. H. (2013). Dynamic Neurovascular Coupling and Uncoupling during Ictal Onset, Propagation, and Termination Revealed by Simultaneous In Vivo Optical Imaging of Neural Activity and Local Blood Volume. *Cerebral Cortex (New York, NY)*, *23*(4), 885–899. https://doi.org/10.1093/cercor/bhs079

Martin, C., Martindale, J., Berwick, J., & Mayhew, J. (2006). Investigating neural–hemodynamic coupling and the hemodynamic response function in the awake rat. *NeuroImage*, *32*(1), 33–48. https://doi.org/10.1016/j.neuroimage.2006.02.021

Mayhew, J., Zheng, Y., Hou, Y., Vuksanovic, B., Berwick, J., Askew, S., & Coffey, P. (1999). Spectroscopic analysis of changes in remitted illumination: the response to increased neural activity in brain. *NeuroImage*, *10*(3 Pt 1), 304–326. https://doi.org/10.1006/nimg.1999.0460

Na, E. S., Nelson, E. D., Kavalali, E. T., & Monteggia, L. M. (2013). The Impact of MeCP2 Loss- or Gain-of-Function on Synaptic Plasticity. *Neuropsychopharmacology*, *38*(1), 212–219. https://doi.org/10.1038/npp.2012.116

Nan, X., Campoy, F. J., & Bird, A. (1997). MeCP2 Is a Transcriptional Repressor with Abundant Binding Sites in Genomic Chromatin. *Cell*, *88*(4), 471–481. https://doi.org/10.1016/S0092-8674(00)81887-5

Nemoto, M., Nomura, Y., Sato, C., Tamura, M., Houkin, K., Koyanagi, I., & Abe, H. (1999). Analysis of Optical Signals Evoked by Peripheral Nerve Stimulation in Rat Somatosensory Cortex: Dynamic Changes in Hemoglobin Concentration and Oxygenation. *Journal of Cerebral Blood Flow & Metabolism*, *19*(3), 246–259. https://doi.org/10.1097/00004647-199903000-00002

Paasonen, J., Salo, R. A., Shatillo, A., Forsberg, M. M., Närväinen, J., Huttunen, J. K., & Gröhn, O. (2016). Comparison of seven different anesthesia protocols for nicotine pharmacologic magnetic resonance imaging in rat. *European Neuropsychopharmacology*, *26*(3), 518–531. https://doi.org/10.1016/j.euroneuro.2015.12.034

Pala, A., & Stanley, G. B. (2022). Ipsilateral Stimulus Encoding in Primary and Secondary Somatosensory Cortex of Awake Mice. *The Journal of Neuroscience: The Official Journal of the Society for Neuroscience*, *42*(13), 2701–2715. https://doi.org/10.1523/JNEUROSCI.1417-21.2022

Pidoux, B., & Verley, R. (1979). Projections on the cortical somatic I barrel subfield from ipsilateral vibrissae in adult rodents. *Electroencephalography and Clinical Neurophysiology*, *46*(6), 715–726. https://doi.org/10.1016/0013-4694(79)90111-1

Plomp, G., Michel, C. M., & Quairiaux, C. (2017). Systematic population spike delays across cortical layers within and between primary sensory areas. *Scientific Reports*, *7*, 15267. https://doi.org/10.1038/s41598-017-15611-2

Purves, D. (2018). *Neuroscience*.

Song, C., Piscopo, D. M., Niell, C. M., & Knöpfel, T. (2018). Cortical signatures of wakeful somatosensory processing. *Scientific Reports*, *8*(1), 11977. https://doi.org/10.1038/s41598-018-30422-9

Tommerdahl, M., Hester, K. D., Felix, E. R., Hollins, M., Favorov, O. V., Quibrera, P. M., & Whitsel, B. L. (2005). Human vibrotactile frequency discriminative capacity after adaptation to 25 Hz or 200 Hz stimulation. *Brain Research*, *1057*(1–2), 1–9. https://doi.org/10.1016/j.brainres.2005.04.031

Trappe, R., Laccone, F., Cobilanschi, J., Meins, M., Huppke, P., Hanefeld, F., & Engel, W. (2001). MECP2 Mutations in Sporadic Cases of Rett Syndrome Are Almost Exclusively of Paternal Origin. *American Journal of Human Genetics*, *68*(5), 1093–1101. https://www.ncbi.nlm.nih.gov/pmc/articles/PMC1226090/

Vanzetta, I., & Grinvald, A. (1999). Increased cortical oxidative metabolism due to sensory stimulation: implications for functional brain imaging. *Science (New York, N.Y.)*, *286*(5444), 1555–1558. https://doi.org/10.1126/science.286.5444.1555

Whitmire, C. J., & Stanley, G. B. (2016). Rapid Sensory Adaptation Redux: A Circuit Perspective. *Neuron*, *92*(2), 298–315. https://doi.org/10.1016/j.neuron.2016.09.046

Zachariah, R. M., Olson, C. O., Ezeonwuka, C., & Rastegar, M. (2012). Novel MeCP2 Isoform-Specific Antibody Reveals the Endogenous MeCP2E1 Expression in Murine Brain, Primary Neurons and Astrocytes. *PLOS ONE*, *7*(11), e49763. https://doi.org/10.1371/journal.pone.0049763

Zucker, R. S., & Regehr, W. G. (2002). Short-term synaptic plasticity. *Annual Review of Physiology*, *64*, 355–405. https://doi.org/10.1146/annurev.physiol.64.092501.114547